Atmos. Chem. Phys. Discuss., 12, 7475–7520, 2012
www.atmos-chem-phys-discuss.net/12/7475/2012/
doi:10.5194/acpd-12-7475-2012

Atmospheric Chemistry and Physics Discussions

Isoprene emissions in Africa inferred from OMI observations of formaldehyde columns

E. A. Marais[1], D. J. Jacob[1,2], T. P. Kurosu[3,*], K. Chance[3], J. G. Murphy[4], C. Reeves[5], G. Mills[5], S. Casadio[6], D. B. Millet[7], M. P. Barkley[8], F. Paulot[2], and J. Mao[9]

[1]Earth and Planetary Sciences, Harvard University, Cambridge, MA, USA
[2]School of Engineering and Applied Sciences, Harvard University, Cambridge, MA, USA
[3]Harvard-Smithsonian Center for Astrophysics, Cambridge, MA, USA
[4]Department of Chemistry, University of Toronto, Toronto, Canada
[5]School of Environmental Sciences, University of East Anglia, Norwich, UK
[6]Instrument Data quality Evaluation and Analysis (IDEAS), Serco Spa Via Sciadonna 24, 00044 Frascati (Roma), Italy
[7]Department of Soil, Water and Climate, University of Minnesota, St. Paul, MN, USA
[8]Space Research Centre, University of Leicester, Leicester, UK
[9]Atmospheric and Oceanic Sciences, Princeton University, Princeton, NJ, USA
[*]now at: Earth Atmosphere Science, Jet Propulsion Laboratory, Pasadena, CA, USA

Received: 21 February 2012 – Accepted: 4 March 2012 – Published: 15 March 2012

Correspondence to: E. A. Marais (emarais@fas.harvard.edu)

Published by Copernicus Publications on behalf of the European Geosciences Union.

ACPD
12, 7475–7520, 2012

Abstract

We use 2005–2009 satellite observations of formaldehyde (HCHO) columns from OMI to infer biogenic isoprene emissions at monthly $1 \times 1^{\circ}$ resolution over the African continent. Our work includes new approaches to remove biomass burning influences using OMI absorbing aerosol optical depth data (to account for transport of fire plumes) and anthropogenic influences using AATSR satellite data for persistent small-flame fires (gas flaring). The resulting biogenic HCHO columns (Ω_{HCHO}) follow closely the distribution of vegetation patterns in Africa. We infer isoprene emission (E_{ISOP}) from the local sensitivity $S = \Delta\Omega_{HCHO}/\Delta E_{ISOP}$ derived with the GEOS-Chem chemical transport model using two alternate isoprene oxidation mechanisms, and verify the validity of this approach using AMMA aircraft observations over West Africa and a longitudinal transect across central Africa. Displacement error (smearing) is diagnosed by anomalously high values of S and the corresponding data are removed. We find significant sensitivity of S to NO_x under low-NO_x conditions that we fit to a linear function of tropospheric column NO_2 from OMI. We estimate a 40 % error in our inferred isoprene emissions under high-NO_x conditions and 40–90 % under low-NO_x conditions. Comparison to the state-of-science MEGAN inventory indicates a large overestimate of central African rainforest emissions in that inventory.

1 Introduction

Isoprene ($CH_2 = C(CH_3)CH = CH_2$) is the dominant non-methane volatile organic compound (NMVOC) emitted by vegetation, accounting for about 50 % of global NMVOC emissions according to current inventories (Guenther et al., 2006). It is a major precursor of organic aerosol (Claeys et al., 2004; Henze and Seinfeld, 2006; Kroll et al., 2006) and of tropospheric ozone (Fiore et al., 2011; Tao et al., 2003; Trainer et al., 1987), thus impacting air quality, climate, and human health. Isoprene also affects the abundance of OH, the main atmospheric oxidant (Lelieveld et al., 2008; Ren et al.,

ACPD
12, 7475–7520, 2012

2008). Satellite observations of formaldehyde (HCHO), a high-yield product of isoprene oxidation, can provide useful constraints on isoprene emissions (Palmer et al., 2003). Here we use HCHO satellite observations from the Ozone Monitoring Instrument (OMI) to better quantify isoprene emissions from the African continent. Africa appears as a major isoprene source region in global HCHO satellite data (Meyer-Arnek et al., 2005; De Smedt et al., 2008), yet it has thus far received little attention.

Isoprene emission inventories in atmospheric chemistry models generally follow the Guenther et al. (1995) framework, which uses base emissions for different ecosystem types modulated by local environmental factors. These inventories are constructed by extrapolation of limited ecosystem data and best understanding of processes, and are commonly called "bottom-up". Arneth et al. (2008) point out that there is considerable uncertainty in bottom-up isoprene emission inventories, more than is apparent from the spread of values in the literature, as all tend to rely on the same limited data and algorithm framework. Direct isoprene emission measurements in Africa are particularly limited, consisting of a few data for tropical rainforests (Greenberg et al., 1999; Klinger et al., 1998; Serça et al., 2001), woodlands (Greenberg et al., 2003, 1999; Otter et al., 2002), savannas (Guenther et al., 1996; Harley et al., 2003; Klinger et al., 1998; Otter et al., 2002; Saxton et al., 2007), and shrublands (Otter et al., 2002).

An alternate "top-down" approach for estimating isoprene emissions is to use HCHO column measurements made by satellites from solar backscatter in the 330–360 nm absorption bands (Chance et al., 2000). Isoprene has an atmospheric lifetime of typically less than 1 h against oxidation by OH, producing HCHO which has a lifetime of 1–2 h against photolysis and oxidation by OH. This adds to the HCHO background originating mainly from the oxidation of methane. Thus the HCHO columns measured from space can be related to the underlying isoprene emission (Palmer et al., 2003). Contributions from other biogenic or anthropogenic NMVOCs are generally much weaker because emissions are lower and/or HCHO production is slower (Palmer et al., 2003). Inference of isoprene emissions from HCHO column measurements by the GOME (1995 launch), SCIAMACHY (2002 launch), and OMI (2004 launch) satellite instruments has

ACPD
12, 7475–7520, 2012

been reported in a number of studies for North America (Abbot et al., 2003; Millet et al., 2008; Palmer et al., 2003, 2006), Asia (Fu et al., 2007), Europe (Curci et al., 2010; Dufour et al., 2009), South America (Barkley et al., 2008), and globally (Shim et al., 2005; Stavrakou et al., 2009b). Biomass burning makes a major seasonal contribution to HCHO in the tropics, and was screened by Barkley et al. (2008) using satellite fire count and NO_2 data.

Relating HCHO columns to isoprene emission requires a quantitative relationship between the two obtained with a chemical transport model (CTM). Most of our current understanding of isoprene chemistry has been developed for high concentrations of nitrogen oxide radicals ($NO_x \equiv NO + NO_2$) that originate in the atmosphere from combustion sources and soil emissions. Under these high-NO_x conditions (>1 ppb NO_x) the organic peroxy radicals (RO_2) produced from isoprene oxidation react preferentially with NO. The resulting HCHO yield is relatively well quantified and is mostly realized in the first stage of isoprene oxidation (Millet et al., 2006; Palmer et al., 2003). Under low-NO_x conditions more typical of Africa, the RO_2 radicals may instead react with HO_2 or isomerize (Peeters et al., 2009), modifying and delaying HCHO yields (Mao et al., 2010; Palmer et al., 2003, 2006). Delay in HCHO production causes smearing in the local relationship between isoprene emission and the HCHO column (Palmer et al., 2003). This smearing can in principle be resolved in a formal inversion accounting for CTM transport (Shim et al., 2005; Stavrakou et al., 2009b), but this requires more confidence than is probably warranted in the coupling between chemical and transport timescales.

Here we use a 5-yr record of OMI HCHO data (2005–2009) to constrain isoprene emissions from the African continent. We convert HCHO columns to isoprene emissions by using the GEOS-Chem CTM with updated isoprene chemistry (Paulot et al., 2009a, b). We introduce a new method to screen biomass burning influence based on OMI observations of aerosol absorption optical depth (AAOD) (Torres et al., 2007) and also screen urban and gas flaring influences. We use aircraft observations from the African Monsoon Multidisciplinary Analysis (AMMA) campaign in West Africa during

ACPD
12, 7475–7520, 2012

July–August 2006 (Murphy et al., 2010; Reeves et al., 2010; Stone et al., 2010) to test the GEOS-Chem simulation of isoprene chemistry and estimate the smearing in the isoprene-HCHO relationship. We also derive a new approach to account for the NO_x dependence of the isoprene-HCHO relationship using OMI NO_2 data.

2 Constructing a data set of OMI biogenic HCHO columns

2.1 Slant columns

The Ozone Monitoring Instrument (OMI) (Levelt et al., 2006) was launched onboard the Aura satellite in 2004. It has spatial resolution of $13 \times 24\,km^2$ at nadir, an equator crossing time of 13:38 LT, and achieves daily global coverage with a cross-track swath width of 2600 km. HCHO slant columns (Ω_s) are a standard product from the OMI instrument, obtained by spectral fitting of backscattered solar radiation in the 327.5–356.5 nm window (http://www.cfa.harvard.edu/atmosphere/Instruments/OMI/PGEReleases/READMEs/OMHCHO_README.pdf). We use OMHCHO Version 2.0 (Collection 3) retrievals for 2005–2009 from the NASA Data and Information Services Center (http://disc.sci.gsfc.nasa.gov/Aura/data-holdings/OMI/omhcho_v003.shtml). We exclude observations that (1) do not pass all fitting and statistical quality checks specified in the standard product (i.e. *MainDataQualityFlag* = 0), (2) have a cloud fraction >0.4 determined from the OMI O_2-O_2 cloud product (Stammes et al., 2008), or (3) are affected by the OMI row anomaly (http://www.knmi.nl/omi/research/product/rowanomaly-background.php).

The OMI data feature a slow increase in the baseline Ω_s with time over 2005–2009 that likely reflects degradation of the instrument. We correct for this using observations over the remote Pacific (40–50° S, 150–160° W) where the OMI data are essentially noise. Following the methodology of Kim et al. (2011) we fit a 4th order polynomial function to the baseline slant column $\Omega_{s,b}$ over that region as a function of time t:

$$\Omega_{s,b} = -2.0 \times 10^3 t^4 + 9.6 \times 10^6 t^3 - 1.3 \times 10^{10} t^2 + 7.5 \times 10^{12} t + 2.5 \times 10^{15} \quad (1)$$

ACPD
12, 7475–7520, 2012

where $\Omega_{s,b}$ is in molecules cm^{-2} and t is in days ($t = 1$ on 1 January 2005). We remove $\Omega_{s,b}$ calculated with Eq. (1) from the OMI measurement of Ω_s and will refer to the residual as Ω_s in what follows.

We thus compile 8-day average values for Ω_s on a $1 \times 1^\circ$ (lat × lon) grid for 2005–2009 (Fig. 1a). The slant column fitting uncertainty for a single observation is 8×10^{15} molecules cm^{-2} on average. 8-day and $1 \times 1^\circ$ averaging reduces the uncertainty to 1–2 × 10^{15} molecules cm^{-2}.

2.2 Removing biomass burning and anthropogenic influences

We remove biomass burning and anthropogenic influences from the Ω_s data in order to isolate the biogenic component. The standard procedure for removing biomass burning is to use space-based observations of fire counts (Barkley et al., 2008; Jaeglé et al., 2005). We begin with this approach by using MODIS day and night fire counts from the Terra satellite. The data are provided daily at a resolution of 1×1 km^2 (Giglio et al., 2003) and we average them for 8 days on the same $1 \times 1^\circ$ grid as Ω_s. We exclude persistent fires associated with large industrial and urban areas of Cairo (Egypt), the Mpumalanga Highveld region (South Africa), and the Niger Delta (Nigeria). We then remove as contaminated by biomass burning all gridsquares with non-zero fire counts for the concurrent and preceding 8-day periods.

Screening only on the basis of fire counts is insufficient as it does not account for the long-range transport of HCHO in biomass burning plumes. Plume influences on HCHO far downwind of fires in Africa are evident from Lagrangian analyses of satellite data (Meyer-Arnek et al., 2005) and AMMA aircraft data (Janicot et al., 2008; Mari et al., 2008; Murphy et al., 2010; Reeves et al., 2010). Solar backscatter satellite instruments retrieve both HCHO and NO_2, and Barkley et al. (2008) previously used NO_2 as an additional filter to screen against biomass burning in tropical South America. We find that this filter is inadequate for Africa because the atmospheric lifetime of NO_x emitted from biomass burning is only a few hours whereas the influence of fires on HCHO is

ACPD
12, 7475–7520, 2012

more sustained owing to continued oxidation of precursor NMVOCs (Alvarado et al., 2010; Hobbs et al., 1996; Trentmann et al., 2003).

Our method to diagnose biomass burning plumes is to use the AAOD product from OMI for the same scenes as HCHO (Torres et al., 2007). Absorbing aerosol is conserved in the plume in the absence of precipitation. We use the level 2 version 3 gridded OMI AAOD product (http://disc.sci.gsfc.nasa.gov/Aura/data-holdings/OMI/omaeruvg_v003.shtml), provided at $0.25 \times 0.25^{\circ}$ horizontal resolution, and average it over 8-day periods on the same $1 \times 1^{\circ}$ grid as Ω_s. The product includes separate contributions from dust and smoke aerosol but separation between the two can be difficult (Ahn et al., 2008) and we find that smoke AAOD is elevated in dusty regions. To address this problem, we subdivide the continent latitudinally into the Mediterranean strip (north of 20° N), northern Africa (4–19° N), equatorial Africa (5° S–4° N), and southern Africa (south of 5° S). For each region we plot the 5-yr frequency distribution of OMI smoke AAOD, as shown in Fig. 2 for southern Africa. This separates biomass burning and non-biomass burning scenes into two populations, and we remove the biomass burning scenes. The smoke AAOD thresholds are 0.02, 0.07, 0.05, and 0.04 for the Mediterranean strip, northern Africa, equatorial Africa, and southern Africa, respectively.

Large dust influence is also problematic in the interpretation of HCHO slant columns because of scattering and absorption by the dust. Northern and equatorial Africa can be very dusty. We filter out high dust scenes with the OMI dust AAOD product previously described using a threshold value of 0.1, above which the radiative interference would be of concern.

The OMI HCHO data show high values over Nigeria (Fig. 1a) that may reflect urban NMVOC emissions in Lagos (Hopkins et al., 2009; Oketola and Osibanjo, 2007; Reeves et al., 2010), biofuel use that is particularly dense in rural Nigeria (Yevich and Logan, 2003), and gas flaring in the Niger Delta (Casadio et al., 2011). Other African countries that practice gas flaring related to the oil and gas industry include Libya, Algeria, Angola, Egypt, Gabon, Sudan, Congo and Tunisia (Casadio et al., 2011). We

ACPD
12, 7475–7520, 2012

remove HCHO associated with gas flaring by using gas flare hotspots retrieved in the 1.6 µm band (Algorithm3 or ALGO3) from the Advanced Along Track Scanning Radiometer (AATSR) satellite instrument (Casadio et al., 2011). We average the AATSR fire counts over the same $1 \times 1^{\circ}$ grid and 8-day averaging period as OMI and remove gridsquares with non-zero gas flares. Over Nigeria the enhancements in HCHO occur beyond the region of flaring, which may reflect pollution transport as well as Lagos emissions and intense biofuel use. We therefore remove a more extensive $3 \times 3^{\circ}$ area around the gridsquares affected by flaring in Nigeria. The AATSR data do not extend over South Africa due to noise from the South Atlantic Anomaly (Casadio et al., 2011), but we find that the six oil refineries in South Africa (SAPIA, 2008) are not associated with elevated HCHO in the OMI data of Fig. 1a. We therefore see no need for additional screening.

Our filtering scheme to remove biomass burning, dust, and anthropogenic contributions from the OMI Ω_s observations is summarized in Fig. 3. It removes 40 % of observations over Africa on average and 70–80 % in the Southern Hemisphere during the dry season. Figure 1 shows the mean OMI Ω_s observations for 2005–2009 before (a) and after (b) application of the filtering scheme. The filtered observations are taken to represent biogenic HCHO in what follows.

2.3 Conversion to vertical columns

The slant column Ω_s obtained by spectral fitting is related to the true vertical column Ω_{HCHO} by an air mass factor ($AMF = \Omega_s/\Omega_{HCHO}$) obtained with a radiative transfer model. We use the formulation of Palmer et al. (2001), which calculates the AMF as the vertical integral of the relative vertical distribution of HCHO (shape factor) weighted by altitude-dependent coefficients (scattering weights). The scattering weights are functions of viewing geometry, surface albedo, and atmospheric scattering by air molecules, aerosols, and clouds. Cloud fraction and cloud top pressure are from the OMI O_2-O_2 cloud product (Stammes et al., 2008). The LIDORT radiative transfer model (Spurr et al., 2001) is used to calculate scattering weights for individual scenes. Clouds are

ACPD
12, 7475–7520, 2012

represented by Lambertian surfaces with an albedo of 0.8, as recommended by Koelemeijer and Stammes (1999), and consistent with the O_2-O_2 cloud algorithm. Surface albedo for the African continent is from the OMI reflectance climatology at 345 nm (Kleipool et al., 2008). HCHO and aerosol vertical distributions are monthly mean values from the GEOS-Chem CTM, described in Sect. 3.

We find that 62 % of the spatial variability in the annual average AMFs over Africa is driven by OMI surface albedo. The AMF is close to unity for much of the continent (average 1.2), with larger values over the Sahara and Namib Deserts (high albedo) and lower values over central Africa (low albedo). Figure 1c shows the resulting annual mean distribution of HCHO vertical columns Ω_{HCHO}. We see that most of the variability in Ω_{HCHO} is present in the slant column data and thus is not driven by the AMF. The Ω_{HCHO} patterns match closely the distribution of major land types in Africa (Fig. 1d), supporting the interpretation of HCHO as a proxy for isoprene emission. Maximum values are found over evergreen broadleaf forests in the tropics. Low values occur over barren, shrub, herbaceous, and cultivated vegetation. Small-scale biogenic features are apparent such as the forested belt along the east coast of South Africa, crops along the Nile River, and the coastal vegetated Mediterranean strip.

3 GEOS-Chem model

3.1 General description

We use the GEOS-Chem global 3-D CTM (version 8-03-01, http://geos-chem.org) to (1) estimate the vertical distribution of HCHO for use in the AMF calculation and (2) quantify the relationship between isoprene emissions and HCHO column abundance. GEOS-Chem is driven by Goddard Earth Observing System (GEOS-5) assimilated meteorological data from the NASA Global Modeling and Assimilation Office (GMAO). The GEOS-5 meteorological data have a native horizontal resolution of $0.5 \times 0.67^{\circ}$ with 72 vertical pressure levels and 6-h temporal frequency (3-h for surface

ACPD
12, 7475–7520, 2012

variables and mixing depths). We use data for year 2006 and degrade the horizontal resolution to $2 \times 2.5^{\circ}$ for input to GEOS-Chem. The model results presented here are from one year of simulation (2006) following one year of spinup for chemical initialization.

Biogenic emission of isoprene is calculated locally in GEOS-Chem using the MEGAN v2.1 inventory (Guenther et al., 2006), with modifications described below. Anthropogenic emissions of NO_x in Africa are from the EDGAR v2.0 inventory (Olivier et al., 1996). Biomass burning NMVOC and NO_x emissions are from the Global Fire Emissions Database v2 (van der Werf et al., 2006). NO_x emissions from soils and fertilizer use are from the algorithm of Yienger and Levy (1995) as implemented by Wang et al. (1998).

Dry deposition in GEOS-Chem follows the standard resistance-in-series scheme of Wesely (1989). In that scheme, gases are deposited as determined by their Henry's law solubility and their surface reactivity (referenced to ozone). Here we have updated the dry deposition of HCHO and other oxygenated products of isoprene oxidation including methyl vinyl ketone (MVK), methacrolein (MACR), glycolaldehyde, and dicarbonyls to have the same surface reactivity as ozone, based on observational evidence of rapid deposition (Karl et al., 2004, 2009; Misztal et al., 2010; Pugh et al., 2010; Sumner et al., 2001) and following the recommendation of Karl et al. (2010). We also include in the model wet and dry deposition of isoprene peroxides and epoxydiols using respective Henry's law constants of 1.7×10^6 M atm^{-1} (US EPA, 2011) and 1.3×10^8 M atm^{-1} (Eddingsaas et al., 2010).

We account in this GEOS-Chem version for the grid-scale transport of isoprene peroxides produced from oxidation of isoprene under low-NO_x conditions. Previous versions of GEOS-Chem did not include this transport, leading to an underestimate in the spatial displacement (smearing) between isoprene emission and the resulting HCHO columns.

ACPD
12, 7475–7520, 2012

3.2 Improved treatment of isoprene chemistry

GEOS-Chem includes detailed ozone-NO_x-VOC-aerosol coupled chemistry originally described by Bey et al. (2001) and Park et al. (2004), with recent updates described by Mao et al. (2010). We have updated the rate coefficients for the reactions of HO_2 with $>C_2$ peroxy radicals to Eq. (iv) of Saunders et al. (2003). At 298 K the rate coefficient doubles from 0.8 to 1.6×10^{-11} cm^3 $molecule^{-1}$ s^{-1} relative to previous versions of GEOS-Chem, increasing the relative importance of the low-NO_x isoprene oxidation pathway.

The standard isoprene oxidation scheme used in GEOS-Chem is largely based on Horowitz et al. (1998). As with all conventional schemes, it leads to OH titration by isoprene under low-NO_x conditions, but this titration is not seen in observations (Lelieveld et al., 2008; Ren et al., 2008). We implement as an alternate isoprene oxidation scheme in GEOS-Chem the Paulot et al. (2009b) mechanism, where regeneration of OH under low-NO_x conditions takes place via oxidation of epoxydiol species produced from oxidation of isoprene hydroperoxides. Isomerization of the isoprene peroxy radicals leading to the formation of hydroperoxyaldehydes, described in Peeters et al. (2009) and Peeters and Müller (2010), is not included in our mechanism as further work is required to assess the relative importance of this reaction pathway (Crounse et al., 2011; Taraborelli et al., 2012). We compare below results from the "standard" and "Paulot" schemes to assess the degree of uncertainty in simulating HCHO yields. The "standard" chemistry scheme is that in version 8-03-01 of GEOS-Chem with updated $RO_2 + HO_2$ kinetics as described above.

Figure 4 shows the time-dependent yields of HCHO from isoprene oxidation calculated in the DSMACC box model (Emmerson and Evans, 2009) for the standard and Paulot schemes as implemented in GEOS-Chem with different NO_x levels. Each simulation uses fixed concentrations of O_3 (28 ppbv), CO (150 ppbv), and NO_x (0.01, 0.1, and 1 ppbv). Isoprene is initially 1 ppbv and allowed to decay. The temperature is 298 K. Diurnally varying photolysis frequencies are calculated for clear sky conditions

ACPD
12, 7475–7520, 2012

at the Equator with surface albedo of 0.1 and an ozone column of 260 Dobson units. Under high-NO_x conditions (1 ppbv), we find that the ultimate HCHO yield is approached within a few hours and is similar for both schemes. Under low-NO_x conditions (0.1 ppbv), the ultimate yield is 10–20 % lower and takes 1–2 days to achieve, again with similar values for both schemes. The largest difference is under very low NO_x conditions (0.01 ppbv) where the ultimate yield is 30–40 % lower than under high-NO_x conditions and the timescale for reaching that yield is 5–6 days. The Paulot scheme does not show a shorter timescale for reaching the ultimate yield than the standard scheme, despite higher OH, because it generates more HCHO from later-generation isoprene oxidation products. The implications of these results for the isoprene-HCHO relationship will be discussed further in Sect. 4 in the context of GEOS-Chem results and using OMI NO_2 columns to identify NO_x regimes.

3.3 MEGAN bottom-up isoprene emission inventory

We use the MEGAN algorithm of Guenther et al. (2006) as our best prior emission estimate for isoprene to which the constraints from the OMI HCHO data can be compared. This inventory is widely used in global CTMs. Isoprene accounts for 80 % of biogenic NMVOC emissions on a per-carbon basis in Africa according to MEGAN. The canopy-scale isoprene emission flux, E_{ISOP}, per unit area of Earth surface (atoms C cm^{-2} s^{-1}) is computed as:

$$E_{ISOP} = E_0 \gamma_T \gamma_{AGE} \gamma_{SM} \gamma_{CE}. \quad (2)$$

Here E_0 is the emission at baseline conditions of air temperature (303 K), leaf age (80 % mature, 10 % growing, and 10 % old), soil moisture (0.3 m^3 water m^{-3} soil), light (1500 µmol photons m^{-2} s^{-1}), and leaf area index (LAI = 5). The unitless environmental scaling factors (γ) describe the effects of temperature (T), leaf age (AGE), soil moisture (SM), and canopy radiative environment (CE) on E_0. γ_{CE} includes the effects of both LAI and light. Values of E_0 are specified for five plant functional types (PFTs): broadleaf trees, needleleaf trees, grasses, crops, and shrubs. The global distribution

ACPD
12, 7475–7520, 2012

of PFTs is taken from the biome database of Olson et al. (2001), and the distribution of trees in Africa south of the Equator is overwritten by the regional database of Otter et al. (2003). In GEOS-Chem E_0 is input at $1 \times 1^\circ$ and regridded to $2 \times 2.5^\circ$ resolution prior to estimating E_{ISOP}.

Our GEOS-Chem simulation uses the environmental scaling factors γ as given by Guenther et al. (2006) and applied to the local GEOS-5 surface data, except for soil moisture. Stavrakou et al. (2009b) found in their analysis of GOME and SCIAMACHY HCHO satellite data that water stress is an important contributor to variability of isoprene emissions over southern Africa and is not well represented in MEGAN. We use here the soil moisture parameterization developed by Müller et al. (2008) and found by Ferreira et al. (2010) to achieve a good simulation of isoprene emission over West Africa during AMMA:

$$\gamma_{\mathrm{SM}} = \sum_{i=1}^{n} \left[f_i \times \max\left(0, \min\left(1, \frac{(\theta_i - \theta_{i,w})}{0.06}\right)\right)\right], \quad (3)$$

where the summation is over n vertical soil layers, f_i is the root fraction within soil layer i such that $\sum_{i=1}^{n} f_i = 1$, θ_i is the degree of saturation or volumetric ratio of soil moisture to the porosity of the soil (m^3 water m^{-3} air), and $\theta_{i,w}$ is the degree of saturation at the wilting point. The GEOS-5 meteorological data provide θ_i for two layers ($n = 2$): a top soil layer (2 cm) and a root zone layer (1 m). Müller et al. (2008) used a fixed wilting point value of 0.171, but here we use gridded monthly average wilting points, ranging from 0.05 to 0.6 in Africa, from the GEOS-5 catchment land surface model (Koster et al., 2000). We determine f_i within each layer using the parameterization of Zeng (2001) for dominant IGBP landcover types at $1 \times 1^\circ$ from the MODIS landcover data set (Friedl et al., 2002).

Our resulting global emission of isoprene in GEOS-Chem for 2006 is 470 Tg C a^{-1}, within the 440–660 Tg C a^{-1} range given by Guenther et al. (2006). Africa accounts for 20 % of global isoprene emissions. Implementation of the soil moisture scaling factor

ACPD
12, 7475–7520, 2012

γ_{SM} as described above reduces annual isoprene emissions by about 10 % globally and 15 % over Africa. The global reduction in isoprene emissions is less than the 30 % reduction obtained by Müller et al. (2008), likely due to the spatially variable wilting points used here.

4 HCHO-isoprene relationship

Previous interpretation of the HCHO column Ω_{HCHO} in terms of isoprene emission using GEOS-Chem has relied on a local linear regression between the two quantities in the model (Palmer et al., 2003):

$$\Omega_{HCHO} = SE_{ISOP} + B \quad (4)$$

where S is the slope of the reduced-major-axis regression line and B is the intercept representing the background HCHO column. The value of S is determined by the HCHO yield from isoprene oxidation and by the HCHO lifetime. Millet et al. (2008) presented estimates of S for North America in summer by performing either a single regression for the ensemble of GEOS-Chem gridsquares covering North America or local regressions for individual $2 \times 2.5^{\circ}$ gridsquares. The first method yielded $S = 2.4 \times 10^3$ s with high correlation ($R^2 = 0.82$), while the second yielded variable slopes with an interquartile range of $2.0–3.0 \times 10^3$ s. These values were consistent with observation-based estimates for the PROPHET forest site in Michigan (2.1×10^3 s) and INTEX-A aircraft observations over the eastern US (2.3×10^3 s) (Millet et al., 2006; Palmer et al., 2003). Over tropical South America where NO_x levels are much lower, Barkley et al. (2008) found a strong spatial correlation ($R^2 > 0.7$) between E_{ISOP} and Ω_{HCHO} in GEOS-Chem but with large seasonal variability in S – ranging from 1×10^3 s in January–March to 2×10^3 s in May–July.

Here we use our updated version of GEOS-Chem, together with observational constraints from AMMA and OMI, to examine the local E_{ISOP}-Ω_{HCHO} relationships over Africa and their suitability for inferring isoprene emissions from the HCHO column data.

ACPD
12, 7475–7520, 2012

We quantify the smearing of the relationship caused by delay in HCHO production from isoprene, develop a parameterization for the dependence of the E_{ISOP}-Ω_{HCHO} relationship on NO_x, and estimate the errors in the resulting isoprene emission estimates.

4.1 Smearing

We first examine the extent of smearing in the HCHO-isoprene relationship over Africa using aircraft measurements of isoprene, the sum of MVK and MACR (MVK+MACR), and HCHO concentrations obtained during AMMA in West Africa in July–August 2006 (Murphy et al., 2010; Reeves et al., 2010). The AMMA wet season aircraft campaign (Redelsperger et al., 2006), based in Niamey, Niger, made latitudinal transects across sharp vegetation gradients from ocean to dense woodland to desert (Fig. 5). 19 flights were made from 20 July to 17 August 2006, mainly during daytime hours. Boundary layer winds were prevailingly from the south (West African monsoon) (Janicot et al., 2008). We exclude biomass burning plumes as diagnosed by >250 pptv acetonitrile (Commane et al., 2010; Murphy et al., 2010) as well as the flights of 8 August (Lagos urban plume) and 15 August (mesoscale convective system).

Figure 5 shows the AMMA flight tracks superimposed on a map of MODIS LAI for July–August 2006 (Yang et al., 2006), together with latitudinal profiles of observed and simulated isoprene, MVK+MACR, and HCHO concentrations below 900 hPa. The model is sampled along the flight tracks and at the flight times. Also included in Fig. 5 is the HCHO concentration below 900 hPa inferred from OMI observations for July–August 2005–2009 averaged over the AMMA longitudinal domain (1–4° E) into 1° latitude bins (multi-year temporal averaging is needed to reduce measurement noise). The HCHO concentration below 900 hPa is inferred from OMI HCHO columns by using the mean HCHO vertical profile measured during AMMA (340 pptv above 750 hPa and linear increase from 750 hPa to the surface). The break in the OMI data at 5–7° N reflects systematic exclusion of anthropogenic influence from Nigeria (Sect. 2.2).

The sharp vegetation gradients sampled in AMMA along the direction of the prevailing southerly monsoon winds make the data of great value for understanding smearing

ACPD
12, 7475–7520, 2012

in the HCHO-isoprene relationship. We see from Fig. 5 that observed isoprene and MVK+MACR tightly follow the vegetation gradients, and this is well captured by the model. Model values are much higher than observed at 11–13° N and 7–8° N, reflecting a local overestimate of E_{ISOP} in MEGAN (Ferreira et al., 2010; Murphy et al., 2010). MVK and MACR are first-stage C_4 isoprene oxidation products, with HCHO produced from the additional carbon atom (Paulson et al., 1992). The tightness of the isoprene-(MVK+MACR) relationship in Fig. 5, both in the observations and the model, demonstrates that there is no significant smearing and provides an important test of the isoprene oxidation scheme. Model isoprene concentrations are lower in the Paulot scheme because of OH regeneration from the $RO_2 + HO_2$ reaction pathway, as described in Sect. 3.2, but this has negligible impact on the simulation of (MVK+MACR).

The right panel of Fig. 5 shows that observed and simulated HCHO are also strongly correlated with the vegetation gradients. The AMMA observations for HCHO are much lower than the model or inferred from OMI, and we do not have an explanation for this beyond the possibility of large bias in the Hantzsch-fluorometric instrument used on the aircraft (Grossmann et al., 2003; Hak et al., 2005; Klemp et al., 2003; Still et al., 2006). Because HCHO is produced together with MVK+MACR it would be difficult to account for a model bias in HCHO but not in MVK+MACR. Tests with the model indicate little sensitivity to the assumed deposition velocities. In any case, comparison of the HCHO and isoprene latitudinal gradients shows no significant northward smearing either in the observations or the model. The strongest correlation between observed isoprene and HCHO ($R^2 = 0.86$) occurs for an offset of 0.5° north of the peak in observed isoprene (8–12° N). Smearing of ~0.5°, combined with a mean observed southerly wind speed of 17 km h^{-1} south of 12° N, implies a timescale of less than a day for production of HCHO from isoprene.

The negligible smearing in the AMMA observations may reflect the relatively high NO_x conditions. Boundary layer (>900 hPa) NO_x concentrations in the region of isoprene emission (7–13° N) averaged 360 pptv in the observations and 310 pptv in the model, due to a mix of influences from soil, anthropogenic, and distant biomass burning

ACPD
12, 7475–7520, 2012

sources (Hopkins et al., 2009; Reeves et al., 2010; Stewart et al., 2008). We find in GEOS-Chem that such a NO_x concentration places the AMMA conditions at the threshold between the high-NO_x regime (where isoprene RO_2 reacts mainly with NO) and the low-NO_x regime (where isoprene RO_2 reacts mainly with HO_2). Stone et al. (2010) found a 70 % mean contribution of the high-NO_x pathway during AMMA using the DSMACC box model.

The OMI NO_2 data offer a broader perspective on NO_x regimes across Africa. Figure 6 shows annual average tropospheric columns of NO_2 (Ω_{NO_2}) from OMI (Boersma et al., 2007) for 2005–2009 and compares to the GEOS-Chem simulation for 2006. Biomass burning influence has been removed in the observations using MODIS fire counts and OMI AAOD (Sect. 2.2) and in GEOS-Chem with black carbon AOD from the model, for consistency with the removal of biomass burning influence in the OMI HCHO column product. We find from the AMMA observations (Stewart et al., 2008) that, similar to HCHO, NO_2 increases linearly from 750 hPa to the surface. Mean NO_2 observations above 750 hPa are below the limit of detection of the aircraft instrument. Thus 1 ppbv of boundary layer NO_x corresponds roughly to a tropospheric NO_2 column of 2×10^{15} molecules cm^{-2}. The fitting precision of 7–8 $\times 10^{14}$ molecules cm^{-2} for individual OMI NO_2 pixels (Boersma et al., 2007) is reduced to 3–4 $\times 10^{13}$ molecules cm^{-2} for monthly mean data at $1 \times 1^{\circ}$ resolution, so that levels as low as ~0.02 ppbv NO_x are detectable. We see in Fig. 6 that much of Africa is in an intermediate NO_x regime (0.1–1 ppbv). Even in the absence of continental biomass burning influences, significant boundary layer NO_x levels are maintained in Africa by soil emissions (Jaeglé et al., 2005) and by decomposition of peroxyacetylnitrate (PAN) originating from outside the continent (Moore and Remedios, 2010; Singh and Hanst, 1981).

We further examined the effect of high isoprene emissions on smearing as a result of OH titration. For this we consider the equatorial forest of central Africa (3° S–3° N) in July where NO_x levels are moderate (average tropospheric NO_2 columns of 8.4 and 5.7×10^{14} molecules cm^{-2} for OMI and GEOS-Chem, respectively), and ventilation is by a steady easterly wind. Figure 7 shows the longitudinal gradients of MEGAN E_{ISOP},

ACPD
12, 7475–7520, 2012

OMI Ω_{HCHO}, and model column HCHO (standard and Paulot schemes) across the region. Immediately downwind (to the west) of the rainforest is a shadow region where elevated HCHO does not correspond to collocated isoprene emission but instead reflects transport from the forest. Assuming that MEGAN correctly represents the location of isoprene emission (mainly determined by the location of the equatorial rainforest), enhancements in OMI Ω_{HCHO} are sustained ~2–3° west of that location. The smearing is well reproduced by the model using either the standard or Paulot scheme and the extent of smearing is not reduced in the Paulot scheme as a result of OH regeneration. Combined with a mean easterly wind speed of 5 km h^{-1} for the region, it implies a timescale of ~2–3 days for production of HCHO from isoprene. We will see below how we can screen such shadow regions from the dataset.

4.2 NO_x dependence

We now examine the variability of the Ω_{HCHO}-E_{ISOP} relationship over Africa in GEOS-Chem measured by the local slope S in Eq. (4). This variability reflects differences in the chemical environment as well as the effect of smearing in an inhomogeneous isoprene emission field. Millet et al. (2008) previously examined the spatial variability of S over North America by constructing local Ω_{HCHO}-E_{ISOP} regressions at the $2 \times 2.5°$ grid resolution of GEOS-Chem, relying on the temperature-driven day-to-day variation of E_{ISOP} in a given gridsquare to define a dynamic range for the regression. We find that this is not an effective approach in Africa as day-to-day variability in isoprene emission is often small. We derive instead the Ω_{HCHO}-E_{ISOP} relationship in GEOS-Chem by conducting a sensitivity simulation with isoprene emissions reduced by a factor of 2 from the MEGAN values. We then infer $S = \Delta\Omega_{HCHO}/\Delta E_{ISOP}$ for individual gridsquares and months (gridsquare-months) where Δ is the monthly mean change relative to the standard simulation, excluding periods of biomass burning influence (diagnosed with black carbon AOD in the model). Values of S over the southeast US (75–100° W, 27–40° N) for June–August 2006 using this approach are 1.9 and 2.0×10^3 s for the standard and

ACPD
12, 7475–7520, 2012

Paulot schemes, respectively, similar to values reported by Millet et al. (2006, 2008) and Palmer et al. (2006).

Gridsquare-months affected by smearing can be diagnosed in this analysis by anomalously high values of S. We find that 41 % of gridsquare-months in GEOS-Chem over Africa have $S > 4 \times 10^3$ s, which is higher than the HCHO yields from isoprene emission would allow and reflects the effect of smearing mainly in regions where isoprene emissions are close to zero (such as the vast desert expanses as well as coastal gridsquares). Although this may seem like a large population to exclude, the corresponding area accounts for only 2 % of isoprene emission over Africa in MEGAN and thus is largely irrelevant for our purpose. We remove all gridsquare-months in GEOS-Chem with $S > 4 \times 10^3$ s in what follows.

For the remainder of the data we find a significant dependence of S on the local NO_x concentration, as would be expected from our box model results in Fig. 4. We choose to define this relationship in the model in terms of S vs. Ω_{NO_2} so that the OMI Ω_{NO_2} data can be applied to remove the effects of model errors in NO_x. Figure 8 shows the S values calculated for individual $2 \times 2.5^\circ$ gridsquare-months over the African continent in 2006 as a function of local model Ω_{NO_2}. The data are averaged into 1×10^{14} molecules NO_2 cm^{-2} bins. For $\Omega_{NO_2} \leq 1 \times 10^{15}$ molecules cm^{-2} (equivalent to 0.5 ppbv surface NO_x using our conversion factor) we find a linear relationship between S and Ω_{NO_2} ($R^2 > 0.9$) reflecting the increasing importance of the $RO_2 + NO$ pathway with increasing NO_x. For $\Omega_{NO_2} > 1 \times 10^{15}$ molecules cm^{-2} we find that S levels off as the $RO_2 + NO$ pathway becomes dominant. 10–20 % higher HCHO yields in the Paulot scheme compared with the standard scheme are consistent with the box model results of Fig. 4. The average Ω_{NO_2} inferred from observations of NO_2 during AMMA is included in Fig. 8 for reference; we see that the AMMA conditions are close to the threshold between high-NO_x and low-NO_x conditions, consistent with Stone et al. (2010) and our earlier discussion.

ACPD
12, 7475–7520, 2012

4.3 Error analysis

Inference of isoprene emission from OMI column HCHO involves a number of steps, all of which are prone to error. Here we estimate these different error terms and their contributions to the overall error.

The spectral fitting uncertainty for Ω_s observations averaged over $1 \times 1^\circ$ gridsquares and 8-day periods is $1–2 \times 10^{15}$ molecules cm^{-2} (Sect. 2.1). We find (not shown) that the model can reproduce the shape of the mean HCHO vertical profile observed in AMMA (linear decrease from the surface to 750 hPa, low values above 750 hPa), suggesting that there is no particular problem in simulating the HCHO vertical shape factor under African conditions. In the absence of better information, we adopt the AMF error estimate of Millet et al. (2006) derived from aircraft observations in North America: 15 % for clear sky increasing to 24 % for 50 % cloud cover (Millet et al., 2006). Taking a fitting error of 2×10^{15} molecules cm^{-2} and an AMF error of 20 % (since we exclude scenes with >40 % cloud cover), and applying these errors in quadrature to a vertical HCHO column of 1×10^{16} molecules cm^{-2} with AMF of 1.2, we estimate an overall error on the OMI HCHO retrieval of 2×10^{15} molecules cm^{-2} or 20 %.

Conversion of HCHO columns to isoprene emission using Eq. (4) involves errors in the slope S due both to the chemical mechanism and to smearing. Figure 8 shows that the standard and Paulot mechanisms differ by only 15 % in their calculations of S, which is similar to the error estimates from Palmer et al. (2006) and Millet et al. (2008) in comparing S values from GEOS-Chem to aircraft and surface observations over the US. The error is certainly larger under low-NO_x conditions where better understanding of isoprene chemistry is needed. Still, it appears that the error bars on S shown in Fig. 8 (which we attribute mainly to smearing) are larger than the errors induced by the chemical mechanism. From these error bars we derive an uncertainty in S from smearing of 750 s for the low-NO_x regime ($\Omega_{NO_2} = 0.2–1 \times 10^{15}$ molecules cm^{-2}) and 690 s for the high-NO_x regime ($\Omega_{NO_2} > 1 \times 10^{15}$ molecules cm^{-2}).

ACPD
12, 7475–7520, 2012

Error in the OMI tropospheric NO_2 column (σ_{NO_2}) also propagates to error in the linear regression equation $S = (1600 \pm 160)\ \Omega_{NO_2} + (721 \pm 114)$ for the low-NO_x regime (Paulot scheme in Fig. 8). We use the expression from Boersma et al. (2008) to estimate σ_{NO_2} for 8-day average Ω_{NO_2} observations:

$$\sigma_{NO_2} = \frac{1.0 \times 10^{15} + 0.3 \times \Omega_{NO_2}}{\sqrt{8} \times \sqrt{3.5}}, \quad (5)$$

and propagate this with the linear regression errors in the slope m ($\sigma_m = 160$) and intercept c ($\sigma_c = 114$). The resulting error standard deviation σ_S in S is determined as $\sigma_S = \sqrt{\left(m \times \sigma_{NO_2}\right)^2 + \left(\Omega_{NO_2} \times \sigma_m\right)^2 + \sigma_c^2}$ and is in the range 340–440 s for Ω_{NO_2} of 0.2–1.0 $\times 10^{15}$ molecules cm^{-2}; smaller than the estimated smearing error of 750 s. The error in S at low NO_x, adding in quadrature the contributions from smearing and from the linear regression of S against Ω_{NO_2}, is 823–870 s (35–84 %).

The overall error in inferring isoprene emission from OMI HCHO columns, adding in quadrature the errors on the OMI retrieval of HCHO columns and the conversion of HCHO columns to isoprene emission, is 40 % in the high-NO_x regime and 40–90 % in the low-NO_x regime. These errors apply to 8-day average $1 \times 1^\circ$ OMI HCHO data and could be reduced by further temporal averaging to the extent that they are random, which is difficult to assess given the uncertainties associated with the isoprene oxidation mechanism at low levels of NO_x.

5 Implications for OMI-derived isoprene emissions in Africa

We have presented here a new methodology for inferring isoprene emissions from HCHO satellite data and applied it to the African continent using OMI. Detailed discussion of the implications for African isoprene emissions and their dependence on environmental variables is left to a separate paper. We present here some preliminary

ACPD
12, 7475–7520, 2012

results. For this purpose we use the 2005–2009 monthly mean OMI HCHO vertical columns at $1 \times 1^{\circ}$ horizontal resolution derived in Sect. 2, monthly mean S values computed from GEOS-Chem with the Paulot scheme, and 2005–2009 monthly mean NO_2 tropospheric column observations from OMI (Boersma et al., 2007).

Figure 9 shows the resulting spatial distribution of annual isoprene emissions at 12:00–15:00 local time (LT) and compares to the corresponding values from the MEGAN inventory. Values are means for all $1 \times 1^{\circ}$ gridsquare-months that are not excluded from our analysis because of biomass burning, anthropogenic, dust, or smearing influences. Fully excluded areas are shown in grey. The right panel of Fig. 9 shows the difference between the OMI-derived emissions and values from MEGAN.

From the data in Fig. 9 we find that the annual mean isoprene emissions in Africa inferred from OMI ($60\,Tg\,C\,a^{-1}$) are on average 22 % lower than the MEGAN values ($77\,Tg\,C\,a^{-1}$). Larger regional discrepancies are apparent. For example, OMI is on average 33 % lower than MEGAN over the central African rainforest, while 38 % higher over the southern deciduous broadleaf forests.

6 Conclusions

We presented a new method for inferring biogenic isoprene emissions from satellite observations of HCHO columns under the particularly challenging conditions of the tropics, and applied this method to 2005–2009 OMI HCHO observations over the African continent.

Removing biomass burning influence is critical for isolating the biogenic component of HCHO in the tropics. Previous procedures using satellite fire counts or NO_2 columns are insufficient because they do not account for long-range transport of fire plumes. Here we used OMI observations of absorbing aerosol optical depth (AAOD) as an additional screening tool. We also identified a significant anthropogenic component over Africa associated with gas flaring, particularly in Nigeria, and removed it

ACPD
12, 7475–7520, 2012

using small-flame satellite fire data. Our resulting biogenic HCHO product shows close correspondence with the distribution of vegetation in Africa.

Inferring isoprene emission from HCHO column data requires knowledge of the time-dependent HCHO yield from isoprene oxidation. This is a challenge in the tropics because of the prevailing low-NO_x conditions under which the isoprene oxidation mechanism is not well understood and HCHO production may be delayed. Here we used two alternate mechanisms to quantify HCHO-isoprene relationships in GEOS-Chem. The two mechanisms show a similar positive NO_x dependence of the HCHO yield under low-NO_x conditions, and a delay between isoprene emission and HCHO production ranging from less than a day under high-NO_x conditions to several days under low-NO_x conditions. This delay smears the local relationship between isoprene emission (E_{ISOP}) and HCHO columns (Ω_{HCHO}).

We evaluated the GEOS-Chem simulation of the HCHO-isoprene relationship using aircraft observations from the AMMA campaign along a latitudinal transect of vegetation types in West Africa. Both observations and model show strong spatial correlation between isoprene, MVK+MACR (first-stage products of isoprene oxidation associated with HCHO formation), and HCHO. This implies insignificant (<100 km) smearing in the HCHO-isoprene relationship. Inspection of longitudinal gradients across the equatorial forest of central Africa, where NO_x is low, indicates smearing of ~200–300 km. This means that large isoprene source regions under low-NO_x conditions produce a shadow effect downwind that affects interpretation of the local HCHO-isoprene relationship.

We computed local relationships between HCHO columns and isoprene emission at the $2 \times 2.5^{\circ}$ GEOS-Chem grid resolution and on a monthly basis by conducting a sensitivity simulation with uniformly perturbed isoprene emission and inferring the relationship $S = \Delta\Omega_{HCHO}/\Delta E_{ISOP}$. Smearing was diagnosed by anomalously high S values and the corresponding scenes were excluded from further analysis. We found that S is sensitive to NO_x at levels below 600 pptv (tropospheric NO_2 column $\leq 1 \times 10^{15}$ molecules cm^{-2}). From there we used the OMI NO_2 column observations to diagnose S for the corresponding OMI HCHO data. The error in OMI-derived isoprene

ACPD
12, 7475–7520, 2012

emissions is 40 % at high NO_x and 40–90 % at low NO_x for 8-day $1 \times 1^\circ$ OMI HCHO grid-squares. Smearing makes the largest contribution to the error for both NO_x regimes.

We presented a preliminary comparison of the OMI-derived annual mean isoprene emissions over Africa to the values computed from the bottom-up MEGAN inventory used in GEOS-Chem. The total OMI-derived isoprene emission for the African continent is 22 % lower than MEGAN. Large regional discrepancies are apparent for the high-emitting evergreen broadleaf trees of central Africa and the Southern Hemisphere deciduous broadleaf trees. In a follow-up paper we will exploit the OMI HCHO data to develop improved understanding of the environmental, seasonal, and interannual variations in isoprene emission over Africa using the OMI HCHO observations.

The two main uncertainties in using space-based HCHO column data to infer isoprene emission are (1) the isoprene oxidation mechanism as it relates to HCHO production under low-NO_x conditions, (2) the coupling between transport and chemistry determining the displacement between observed HCHO columns and precursor isoprene emissions. The latter could be addressed by using a CTM adjoint inversion (Stavrakou et al., 2009b). This will eventually be necessary if we are to exploit the fine resolution of the satellite observations ($13 \times 24\,km^2$ in nadir for OMI) to obtain correspondingly fine constraints on isoprene emission. However, the value of such an approach is hampered at present by inadequate knowledge of the time-dependent HCHO yields from isoprene oxidation under low-NO_x conditions, and by the difficulty of representing the coupling between transport and chemistry over timescales relevant to boundary layer mixing and mesoscale motions. Future progress most critically requires an improved understanding of isoprene oxidation chemistry through laboratory and field measurements.

ACPD
12, 7475–7520, 2012

Acknowledgements. This work was funded by NASA through the Aura Science Team and by a South African National Research Scholarship for Study Abroad to EAM. EAM would like to thank Omar Torres and Folkert Boersma for assistance with OMI satellite products and Sarith Mahanama and Randal Koster for providing updated soil moisture assimilated data over Africa. DBM acknowledges support from NASA ACMAP (#NNX10AG65G).

References

Abbot, D. S., Palmer, P. I., Martin, R. V., Chance, K., Jacob, D. J., and Guenther, A.: Seasonal and interannual variability of North American isoprene emissions as determined by formaldehyde column measurements from space, Geophys. Res. Lett., 30, 1886, doi:10.1029/2003GL017336, 2003.

Ahn, C., Torres, O., and Bhartia, P. K.: Comparison of Ozone Monitoring Instrument UV Aerosol Products with Aqua/Moderate Resolution Imaging Spectroradiometer and Multi-angle Imaging Spectroradiometer observations in 2006, J. Geophys. Res., 113, D16S27, doi:10.1029/2007JD008832, 2008.

Alvarado, M. J., Logan, J. A., Mao, J., Apel, E., Riemer, D., Blake, D., Cohen, R. C., Min, K.-E., Perring, A. E., Browne, E. C., Wooldridge, P. J., Diskin, G. S., Sachse, G. W., Fuelberg, H., Sessions, W. R., Harrigan, D. L., Huey, G., Liao, J., Case-Hanks, A., Jimenez, J. L., Cubison, M. J., Vay, S. A., Weinheimer, A. J., Knapp, D. J., Montzka, D. D., Flocke, F. M., Pollack, I. B., Wennberg, P. O., Kurten, A., Crounse, J., St. Clair, J. M., Wisthaler, A., Mikoviny, T., Yantosca, R. M., Carouge, C. C., and Le Sager, P.: Nitrogen oxides and PAN in plumes from boreal fires during ARCTAS-B and their impact on ozone: an integrated analysis of aircraft and satellite observations, Atmos. Chem. Phys., 10, 9739–9760, doi:10.5194/acp-10-9739-2010, 2010.

Arneth, A., Monson, R. K., Schurgers, G., Niinemets, Ü., and Palmer, P. I.: Why are estimates of global terrestrial isoprene emissions so similar (and why is this not so for monoterpenes)?, Atmos. Chem. Phys., 8, 4605–4620, doi:10.5194/acp-8-4605-2008, 2008.

Barkley, M. P., Palmer, P. I., Kuhn, U., Kesselmeier, J., Chance, K., Kurosu, T. P., Martin, R. V., Helmig, D., and Guenther, A.: Net ecosystem fluxes of isoprene over tropical South America inferred from Global Ozone Monitoring Experiment (GOME) observations of HCHO columns, J. Geophys. Res., 113, D20304, doi:10.1029/2008JD009863, 2008.

ACPD
12, 7475–7520, 2012

Bartholomé, E. and Belward, A. S.: GLC2000: a new approach to global land cover mapping from Earth observation data, Int. J. Remote Sens., 26, 1959–1977, 2005.
Bey, I., Jacob, D. J., Yantosca, R. M., Logan, J. A., Field, B. D., Fiore, A., Li, Q., Liu, H. Y., Mickley, L. J., and Schultz, M. G.: Global modeling of tropospheric chemistry with assimilated meteorology: Model description and evaluation, J. Geophys. Res., 106, 23073–23095, doi:10.1029/2001JD000807, 2001.
Boersma, K. F., Eskes, H. J., Veefkind, J. P., Brinksma, E. J., van der A, R. J., Sneep, M., van den Oord, G. H. J., Levelt, P. F., Stammes, P., Gleason, J. F., and Bucsela, E. J.: Near-real time retrieval of tropospheric NO_2 from OMI, Atmos. Chem. Phys., 7, 2103–2118, doi:10.5194/acp-7-2103-2007, 2007.
Boersma, K., Jacob, D. J., Eskes, H. J., Pinder, R. W., Wang, J., and van der A, R. J.: Intercomparison of SCIAMACHY and OMI tropospheric NO_2 columns: Observing the diurnal evolution of chemistry and emissions from space, J. Geophys. Res., 113, D16S26, doi:10.1029/2007JD008816, 2008.
Casadio, S., Arino, O., and Serpe, D.: Gas flaring monitoring from space using the ATSR instrument series, Remote Sens. Environ., 116, 239–249, doi:10.1016/j.rse.2010.11.022, 2011.
Chance, K., Palmer, P. I., Spurr, R. J. D., Martin, R. V., Kurosu, T. P., and Jacob, D. J.: Satellite observations of formaldehyde over North America from GOME, Geophys. Res. Lett., 27, 3461–3464, doi:10.1029/2000GL011857, 2000.
Claeys, M., Graham, B., Vas, G., Wang, W., Vermeylen, R., Pashynska, V., Cafmeyer, J., Guyon, P., Andreae, M. O., Artaxo, P., and Maenhaut, W.: Formation of secondary organic aerosols through photooxidation of isoprene, Science, 303, 1173–1176, 2004.
Commane, R., Floquet, C. F. A., Ingham, T., Stone, D., Evans, M. J., and Heard, D. E.: Observations of OH and HO_2 radicals over West Africa, Atmos. Chem. Phys., 10, 8783–8801, doi:10.5194/acp-10-8783-2010, 2010.
Crounse, J. D., Paulot, F., Kjaergaard, H. G., and Wennberg, P. O.: Peroxy radical isomerization in the oxidation of isoprene, Phys. Chem. Chem. Phys., 13, 13607–13613, 2011.
Curci, G., Palmer, P. I., Kurosu, T. P., Chance, K., and Visconti, G.: Estimating European volatile organic compound emissions using satellite observations of formaldehyde from the Ozone Monitoring Instrument, Atmos. Chem. Phys., 10, 11501–11517, doi:10.5194/acp-10-11501-2010, 2010.
De Smedt, I., Müller, J.-F., Stavrakou, T., van der A, R., Eskes, H., and Van Roozendael, M.:

ACPD
12, 7475–7520, 2012

Twelve years of global observations of formaldehyde in the troposphere using GOME and SCIAMACHY sensors, Atmos. Chem. Phys., 8, 4947–4963, doi:10.5194/acp-8-4947-2008, 2008.

Dufour, G., Wittrock, F., Camredon, M., Beekmann, M., Richter, A., Aumont, B., and Burrows, J. P.: SCIAMACHY formaldehyde observations: constraint for isoprene emission estimates over Europe?, Atmos. Chem. Phys., 9, 1647–1664, doi:10.5194/acp-9-1647-2009, 2009.

Eddingsaas, N. C., VanderVelde, D. G., and Wennberg, P. O.: Kinetics and products of the acid-catalyzed ring-opening of atmospherically relevant butyl epoxy alcohols, J. Phys. Chem. A, 114, 8106–8113, 2010.

Emmerson, K. M. and Evans, M. J.: Comparison of tropospheric gas-phase chemistry schemes for use within global models, Atmos. Chem. Phys., 9, 1831–1845, doi:10.5194/acp-9-1831-2009, 2009.

Ferreira, J., Reeves, C. E., Murphy, J. G., Garcia-Carreras, L., Parker, D. J., and Oram, D. E.: Isoprene emissions modelling for West Africa: MEGAN model evaluation and sensitivity analysis, Atmos. Chem. Phys., 10, 8453–8467, doi:10.5194/acp-10-8453-2010, 2010.

Fiore, A. M., Levy II, H., and Jaffe, D. A.: North American isoprene influence on intercontinental ozone pollution, Atmos. Chem. Phys., 11, 1697–1710, doi:10.5194/acp-11-1697-2011, 2011.

Friedl, M. A., McIver, D. K., Hodges, J. C. F., Zhang, X. Y., Muchoney, D., Strahler, A. H., Woodcock, C. E., Gopal, S., Schneider, A., Cooper, A., Baccini, A., Gao, F., and Schaaf, C.: Global land cover mapping from MODIS: algorithms and early results, Remote Sens. Environ., 83, 287–302, 2002.

Fu, T.-M., Jacob, D. J., Palmer, P. I., Chance, K., Wang, Y. X., Barletta, B., Blake, D. R., Stanton, J. C., and Pilling, M. J.: Space-based formaldehyde measurements as constraints on volatile organic compound emissions in east and south Asia and implications for ozone, J. Geophys. Res., 112, D06312, doi:10.1029/2006JD007853, 2007.

Giglio, L., Descloitres, J., Justice, C. O., and Kaufman, Y. J.: An enhanced contextual fire detection algorithm for MODIS, Remote Sens. Environ., 87, 273–282, 2003.

Greenberg, J. P., Guenther, A., Madronich, S., Baugh, W., Ginoux, P., Druilhet, A., Delmas, R., and Delon, C.: Biogenic volatile organic compound emissions in central Africa during the Experiment for the Regional Sources and Sinks of Oxidants (EXPRESSO) biomass burning season, J. Geophys. Res., 104, 30659–30671, doi:10.1029/1999JD900475, 1999.

Greenberg, J. P., Guenther, A. B., Harley, P., Otter, L., Veenendaal, E. M., Hewitt, C.

ACPD
12, 7475–7520, 2012

N., James, A. E., and Owen, S. M.: Eddy flux and leaf-level measurements of biogenic VOC emissions from mopane woodland of Botswana, J. Geophys. Res., 108, 8466, doi:10.1029/2002JD002317, 2003.

Grossmann, D., Moorgat, G. K., Kibler, M., Schlomski, S., Bächman, K., Alicke, B., Geyer, A., Platt, U., Hammer, M.-U., Vogel, B., Mihelcic, A., Hofzumahaus, A., Holland, F., and Volz-Thomas, A.: Hydrogen peroxide, organic peroxides, carbonyl compounds, and organic acids measured at Pabstthum during BERLIOZ, J. Geophys. Res., 108, 8250, doi:10.1029/2001JD001096, 2003.

Guenther, A., Hewitt, C. N., Erickson, D., Fall, R., Geron, C., Graedel, T., Harley, P., Klinger, L. F., Lerdau, M., McKay, W. A., Pierce, T., Scholes, B., Steinbrecher, R., Tallamraju, R., Taylor, J., and Zimmerman, P.: A global model of natural volatile organic compound emissions, J. Geophys. Res., 100, 8873–8892, doi:10.1029/94JD02950, 1995.

Guenther, A., Otter, L., Zimmerman, P., Greenberg, J., Scholes, R., and Scholes, M.: Biogenic hydrocarbon emissions from southern African savannas, J. Geophys. Res., 101, 25859–25865, doi:10.1029/96JD02597, 1996.

Guenther, A., Karl, T., Harley, P., Wiedinmyer, C., Palmer, P. I., and Geron, C.: Estimates of global terrestrial isoprene emissions using MEGAN (Model of Emissions of Gases and Aerosols from Nature), Atmos. Chem. Phys., 6, 3181–3210, doi:10.5194/acp-6-3181-2006, 2006.

Hak, C., Pundt, I., Trick, S., Kern, C., Platt, U., Dommen, J., Ordóñez, C., Prévôt, A. S. H., Junkermann, W., Astorga-Lloréns, C., Larsen, B. R., Mellqvist, J., Strandberg, A., Yu, Y., Galle, B., Kleffmann, J., Lörzer, J. C., Braathen, G. O., and Volkamer, R.: Intercomparison of four different in-situ techniques for ambient formaldehyde measurements in urban air, Atmos. Chem. Phys., 5, 2881–2900, doi:10.5194/acp-5-2881-2005, 2005.

Harley, P., Otter, L., Guenther, A., and Greenberg, J.: Micrometeorological and leaf-level measurements of isoprene emissions from a southern African savanna, J. Geophys. Res., 108, 8468, doi:10.1029/2002JD002592, 2003.

Henze, D. K. and Seinfeld, J. H.: Global secondary organic aerosol from isoprene oxidation, Geophys. Res. Lett., 33, L09812, doi:10.1029/2006GL025976, 2006.

Hobbs, P. V., Reid, J. S., Herring, J. A., Nance, J. D., Weiss, R. E., Ross, J. L., Hegg, D. A., Ottmar, R. D., and Liousse, C.: Particle and trace-gas measurements in the smoke from prescribed burns of forest products in the Pacific Northwest, in: Biomass Burning and Global Change, edited by: Levine, J. S., MIT Press, Cambridge, MA., 697–715, 1996.

ACPD
12, 7475–7520, 2012

Hopkins, J. R., Evans, M. J., Lee, J. D., Lewis, A. C., Marsham, J. H., McQuaid, J. B., Parker, D. J., Stewart, D. J., Reeves, C. E., and Purvis, R. M.: Direct estimates of emissions from the megacity of Lagos, Atmos. Chem. Phys., 9, 8471–8477, doi:10.5194/acp-9-8471-2009, 2009.

Horowitz, L. W., Liang, J., Gardner, G. M., and Jacob, D. J.: Export of reactive nitrogen from North America during summertime: Sensitivity to hydrocarbon chemistry, J. Geophys. Res., 103, 13451–13476, doi:10.1029/97JD03142, 1998.

Jaeglé, L., Steinberger, L., Martin, R. V., and Chance, K.: Global partitioning of NO_x sources using satellite observations: Relative roles of fossil fuel combustion, biomass burning and soil emissions, Faraday Discuss., 130, 407–423, 2005.

Janicot, S., Thorncroft, C. D., Ali, A., Asencio, N., Berry, G., Bock, O., Bourles, B., Caniaux, G., Chauvin, F., Deme, A., Kergoat, L., Lafore, J.-P., Lavaysse, C., Lebel, T., Marticorena, B., Mounier, F., Nedelec, P., Redelsperger, J.-L., Ravegnani, F., Reeves, C. E., Roca, R., de Rosnay, P., Schlager, H., Sultan, B., Tomasini, M., Ulanovsky, A., and ACMAD forecasters team: Large-scale overview of the summer monsoon over West Africa during the AMMA field experiment in 2006, Ann. Geophys., 26, 2569–2595, doi:10.5194/angeo-26-2569-2008, 2008.

Karl, T., Potosnak, M., Guenther, A., Clark, D., Walker, J., Herrick, J. D., and Geron, C.: Exchange processes of volatile organic compounds above a tropical rain forest: Implications for modeling tropospheric chemistry above dense vegetation, J. Geophys. Res., 109, D18306, doi:10.1029/2004JD004738, 2004.

Karl, T., Guenther, A., Turnipseed, A., Tyndall, G., Artaxo, P., and Martin, S.: Rapid formation of isoprene photo-oxidation products observed in Amazonia, Atmos. Chem. Phys., 9, 7753–7767, doi:10.5194/acp-9-7753-2009, 2009.

Karl, T., Harley, P., Emmons, L., Thornton, B., Guenther, A., Basu, C., Turnipseed, A., and Jardine, K.: Efficient atmospheric cleansing of oxidized organic trace gases by vegetation, Science, 330, 816–819, 2010.

Kim, J. H., Kim, S. M., Baek, K. H., Wang, L., Kurosu, T., De Smedt, I., Chance, K., and Newchurch, M. J.: Evaluation of satellite-derived HCHO using statistical methods, Atmos. Chem. Phys. Discuss., 11, 8003–8025, doi:10.5194/acpd-11-8003-2011, 2011.

Kleipool, Q. L., Dobber, M. R., de Haan, J. F., and Levelt, P. F.: Earth surface reflectance climatology from 3 years of OMI data, J. Geophys. Res., 113, D18308, doi:10.1029/2008JD010290, 2008.

ACPD
12, 7475–7520, 2012

Klemp, D., Mannschreck, K., and Mittermaier, B.: Comparison of two different HCHO Measurement Techniques: TDLAS and a commercial Hantzsch Monitor – Results from Long term Measurements in a City Plume during the EVA Experiment, in: Emissions of Air Pollutants – Measurements, Calculations and Uncertainties, edited by: Friedrich, R. and Reis, S., Springer Verlag, 2003.

Klinger, L. F., Guenther, G., Tyndall, G., Zimmerman, P., Bangui, M. M., Moutsamboté, J.-M., and Kenfack, D.: Patterns in volatile organic compound emissions along a savanna-rainforest gradient in central Africa, J. Geophys. Res., 103, 1443–1454, doi:10.1029/97JD02928, 1998.

Koelemeijer, R. B. A. and Stammes, P.: Validation of Global Ozone Monitoring Experiment cloud fractions relevant for accurate ozone column retrieval, J. Geophys. Res., 104, 18801–18814, doi:10.1029/1999JD900279, 1999.

Koster, R. D., Suarez, M. J., Ducharne, A., Stieglitz, M., and Kumar, P.: A catchment-based approach to modeling land surface processes in a general circulation model 1. Model structure, J. Geophys. Res., 105, 24809–24822, doi:10.1029/2000JD900327, 2000.

Kroll, J. H., Ng, N. L., Murphy, S. M., Flagan, R. C., and Seinfeld, J. H.: Secondary organic aerosol formation from isoprene photooxidation, Environ. Sci. Technol., 40, 1869–1877, 2006.

Lelieveld, J., Butler, T. M., Crowley, J. N., Dillon, T. J., Fischer, H., Ganzeveld, L., Harder, H., Lawrence, M. G., Martinez, M., Taraborrelli, D., and Williams, J.: Atmospheric oxidation capacity sustained by a tropical forest, Nature, 452, 737–740, 2008.

Levelt, P. F., van den Oord, G. H. J., Dobber, M. R., Mälkki, A., Visser, H., de Fries, J., Stammes, P., Lundell, J. O. V., and Saari, H.: The ozone monitoring instrument, IEEE T. Geosci. Remote Sens., 44, 1093–1101, 2006.

Manly, B. F. J.: Randomization, bootstrap and Monte Carlo methods in biology, Chapman and Hall, New York, 1997.

Mao, J., Jacob, D. J., Evans, M. J., Olson, J. R., Ren, X., Brune, W. H., St. Clair, J. M., Crounse, J. D., Spencer, K. M., Beaver, M. R., Wennberg, P. O., Cubison, M. J., Jimenez, J. L., Fried, A., Weibring, P., Walega, J. G., Hall, S. R., Weinheimer, A. J., Cohen, R. C., Chen, G., Crawford, J. H., McNaughton, C., Clarke, A. D., Jaeglé, L., Fisher, J. A., Yantosca, R. M., Le Sager, P., and Carouge, C.: Chemistry of hydrogen oxide radicals (HO_x) in the Arctic troposphere in spring, Atmos. Chem. Phys., 10, 5823–5838, doi:10.5194/acp-10-5823-2010, 2010.

ACPD
12, 7475–7520, 2012

Mari, C. H., Cailley, G., Corre, L., Saunois, M., Attié, J. L., Thouret, V., and Stohl, A.: Tracing biomass burning plumes from the Southern Hemisphere during the AMMA 2006 wet season experiment, Atmos. Chem. Phys., 8, 3951–3961, doi:10.5194/acp-8-3951-2008, 2008.
Meyer-Arnek, J., Ladstätter-Weißenmayer, A., Richter, A., Wittrock, F., and Burrows, J. P.: A study of the trace gas columns of O_3, NO_2 and HCHO over Africa in September 1997, Faraday Discuss., 130, 387–405, 2005.
Millet, D. B., Jacob, D. J., Turquety, S., Hudman, R. C., Wu, S., Fried, A., Walega, J., Heikes, B. G., Blake, D. R., Singh, H. B., Anderson, B. E., and Clarke, A. D.: Formaldehyde distribution over North America: Implications for satellite retrievals of formaldehyde columns and isoprene emission, J. Geophys. Res., 111, D24S02, doi:10.1029/2005JD006853, 2006.
Millet, D. B., Jacob, D. J., Boersma, K., Fu, T.-M., Kurosu, T. P., Chance, K., Heald, C. L., and Guenther, A.: Spatial distribution of isoprene emissions from North America derived from formaldehyde column measurements by the OMI satellite sensor, J. Geophys. Res., 113, D02307, doi:10.1029/2007JD008950, 2008.
Misztal, P. K., Owen, S. M., Guenther, A. B., Rasmussen, R., Geron, C., Harley, P., Phillips, G. J., Ryan, A., Edwards, D. P., Hewitt, C. N., Nemitz, E., Siong, J., Heal, M. R., and Cape, J. N.: Large estragole fluxes from oil palms in Borneo, Atmos. Chem. Phys., 10, 4343–4358, doi:10.5194/acp-10-4343-2010, 2010.
Moore, D. P. and Remedios, J. J.: Seasonality of Peroxyacetyl nitrate (PAN) in the upper troposphere and lower stratosphere using the MIPAS-E instrument, Atmos. Chem. Phys., 10, 6117–6128, doi:10.5194/acp-10-6117-2010, 2010.
Murphy, J. G., Oram, D. E., and Reeves, C. E.: Measurements of volatile organic compounds over West Africa, Atmos. Chem. Phys., 10, 5281–5294, doi:10.5194/acp-10-5281-2010, 2010.
Müller, J.-F., Stavrakou, T., Wallens, S., De Smedt, I., Van Roozendael, M., Potosnak, M. J., Rinne, J., Munger, B., Goldstein, A., and Guenther, A. B.: Global isoprene emissions estimated using MEGAN, ECMWF analyses and a detailed canopy environment model, Atmos. Chem. Phys., 8, 1329–1341, doi:10.5194/acp-8-1329-2008, 2008.
Oketola, A. A. and Osibanjo, O.: Estimating sectoral pollution load in Lagos by Industrial Pollution Projection System (IPPS), Sci. Total Environ., 377, 125–141, 2007.
Olivier, J. G. J., Bouwman, A. F., van der Maas, C. W. M., Berdowski, J. J. M., Veldt, C., Bloos, J. P. J., Visschedijk, A. J. H., Zandveld, P. Y. J. and Haverlag, J. L.: Description of EDGAR Version 2.0: A set of global emission inventories of greenhouse gases and ozone-depleting

ACPD
12, 7475–7520, 2012

substances for all anthropogenic and most natural sources on a per country basis and on 1° × 1° grid, Bilthoven, The Netherlands, 1996.
Olson, D. M., Dinerstein, E., Wikramanayake, E. D., Burgess, N. D., Powell, G. V. N., Underwood, E. C., D'amico, J. A., Itoua, I., Strand, H. E., Morrison, J. C., Loucks, C. J., Allnutt, T. F., Ricketts, T. H., Kura, Y., Lamoreux, J. F., Wettengel, W. W., Hedao, P., and Kassem, K. R.: Terrestrial ecoregions of the world: a new map of life on earth, BioScience, 51, 933–938, 2001.
Otter, L. B., Guenther, A., and Greenberg, J.: Seasonal and spatial variations in biogenic hydrocarbon emissions from southern African savannas and woodlands, Atmos. Environ., 36, 4265–4275, 2002.
Otter, L., Guenther, A., Wiedinmyer, C., Fleming, G., Harley, P., and Greenberg, J.: Spatial and temporal variations in biogenic volatile organic compound emissions for Africa south of the equator, J. Geophys. Res., 108, 8505, doi:10.1029/2002JD002609, 2003.
Palmer, P. I., Jacob, D. J., Martin, R. V., Spurr, R. J. D., Kurosu, T. P., Bey, I., Yantosca, R., Fiore, A., and Li, Q.: Air mass factor formulation for spectroscopic measurements from satellites: Application to formaldehyde retrievals from the Global Ozone Monitoring Experiment, J. Geophys. Res., 106, 14539–14550, doi:10.1029/2000JD900772, 2001.
Palmer, P. I., Jacob, D. J., Fiore, A. M., Martin, R. V., Chance, K., and Kurosu, T. P.: Mapping isoprene emissions over North America using formaldehyde column observations from space, J. Geophys. Res., 108, 4180, doi:10.1029/2002JD002153, 2003.
Palmer, P. I., Abbot, D. S., Fu, T.-M., Jacob, D. J., Chance, K., Kurosu, T. P., Guenther, A., Wiedinmyer, C., Stanton, J. C., Pilling, M. J., Pressley, S. N., Lamb, B., and Sumner, A. L.: Quantifying the seasonal and interannual variability of North American isoprene emissions using satellite observations of the formaldehyde column, J. Geophys. Res., 111, D12315, doi:10.1029/2005JD006689, 2006.
Park, R. J., Jacob, D. J., Field, B. D., Yantosca, R. M., and Chin, M.: Natural and transboundary pollution influences on sulfate-nitrate-ammonium aerosols in the United States: Implications for policy, J. Geophys. Res., 109, D15204, doi:10.1029/2003JD004473, 2004.
Paulot, F., Crounse, J. D., Kjaergaard, H. G., Kroll, J. H., Seinfeld, J. H., and Wennberg, P. O.: Isoprene photooxidation: new insights into the production of acids and organic nitrates, Atmos. Chem. Phys., 9, 1479–1501, doi:10.5194/acp-9-1479-2009, 2009a.
Paulot, F., Crounse, J. D., Kjaergaard, H. G., Kürten, A., St Clair, J. M., Seinfeld, J. H., and Wennberg, P. O.: Unexpected epoxide formation in the gas-phase photooxidation of

ACPD
12, 7475–7520, 2012

isoprene, Science, 325, 730–733, 2009b.
Paulson, S. E., Flagan, R. C., and Seinfeld, J. H.: Atmospheric photooxidation of isoprene. I: The hydroxyl radical and ground state atomic oxygen reactions, Int. J. Chem. Kinet., 24, 79–101, 1992.
Peeters, J. and Müller, J.-F.: HO_x radical regeneration in isoprene oxidation via peroxy radical isomerisations. II: experimental evidence and global impact, Phys. Chem. Chem. Phys., 12, 14227–14235, 2010.
Peeters, J., Nguyen, T. L., and Vereecken, L.: HO_x radical regeneration in the oxidation of isoprene, Phys. Chem. Chem. Phys., 11, 5935–5939, 2009.
Pugh, T. A. M., MacKenzie, A. R., Hewitt, C. N., Langford, B., Edwards, P. M., Furneaux, K. L., Heard, D. E., Hopkins, J. R., Jones, C. E., Karunaharan, A., Lee, J., Mills, G., Misztal, P., Moller, S., Monks, P. S., and Whalley, L. K.: Simulating atmospheric composition over a South-East Asian tropical rainforest: performance of a chemistry box model, Atmos. Chem. Phys., 10, 279–298, doi:10.5194/acp-10-279-2010, 2010.
Redelsperger, J.-L., Thorncroft, C. D., Diedhiou, A., Lebel, T., Parker, D. J., and Polcher, J.: African Monsoon Multidisciplinary Analysis (AMMA): An international research project and field campaign, B. Am. Meteorol. Soc., 87, 1739–1746, 2006.
Reeves, C. E., Formenti, P., Afif, C., Ancellet, G., Attié, J.-L., Bechara, J., Borbon, A., Cairo, F., Coe, H., Crumeyrolle, S., Fierli, F., Flamant, C., Gomes, L., Hamburger, T., Jambert, C., Law, K. S., Mari, C., Jones, R. L., Matsuki, A., Mead, M. I., Methven, J., Mills, G. P., Minikin, A., Murphy, J. G., Nielsen, J. K., Oram, D. E., Parker, D. J., Richter, A., Schlager, H., Schwarzenboeck, A., and Thouret, V.: Chemical and aerosol characterisation of the troposphere over West Africa during the monsoon period as part of AMMA, Atmos. Chem. Phys., 10, 7575–7601, doi:10.5194/acp-10-7575-2010, 2010.
Ren, X., Olson, J. R., Crawford, J. H., Brune, W. H., Mao, J., Long, R. B., Chen, Z., Chen, G., Avery, M. A., Sachse, G. W., Barrick, J. D., Diskin, G. S., Huey, L. G., Fried, A., Cohen, R. C., Heikes, B., Wennberg, P. O., Singh, H. B., Blake, D. R., and Shetter, R. E.: HO_x chemistry during INTEX-A 2004: Observation, model calculation, and comparison with previous studies, J. Geophys. Res., 113, D05310, doi:10.1029/2007JD009166, 2008.
Saunders, S. M., Jenkin, M. E., Derwent, R. G., and Pilling, M. J.: Protocol for the development of the Master Chemical Mechanism, MCM v3 (Part A): tropospheric degradation of non-aromatic volatile organic compounds, Atmos. Chem. Phys., 3, 161–180, doi:10.5194/acp-3-161-2003, 2003.

ACPD
12, 7475–7520, 2012

Saxton, J. E., Lewis, A. C., Kettlewell, J. H., Ozel, M. Z., Gogus, F., Boni, Y., Korogone, S. O. U., and Serça, D.: Isoprene and monoterpene measurements in a secondary forest in northern Benin, Atmos. Chem. Phys., 7, 4095–4106, doi:10.5194/acp-7-4095-2007, 2007.
Serça, D., Guenther, A., Klinger, L., Vierling, L., Harley, P., Druilhet, A., Greenberg, J., Baker, B., Baugh, W., Bouka-Biona, C., and Loemba-Ndembi, J.: EXPRESSO flux measurements at upland and lowland Congo tropical forest site, Tellus B, 53, 220–234, 2001.
Shim, C., Wang, Y., Choi, Y., Palmer, P. I., Abbot, D. S., and Chance, K.: Constraining global isoprene emissions with Global Ozone Monitoring Experiment (GOME) formaldehyde column measurements, J. Geophys. Res., 110, D24301, doi:10.1029/2004JD005629, 2005.
Singh, H. B. and Hanst, P. L.: Peroxyacetyl nitrate (PAN) in the unpolluted atmosphere: An important reservoir for nitrogen oxides, Geophys. Res. Lett., 8, 941–944, 1981.
South African Petroleum Industry Association (SAPIA): Annual Report, 2008.
Spurr, R. J. D., Kurosu, T. P., and Chance, K. V.: A linearized discrete ordinate radiative transfer model for atmospheric remote-sensing retrieval, J. Quant. Spectrosc. Ra., 68, 689–735, 2001.
Stammes, P., Sneep, M., de Haan, J. F., Veefkind, J. P., Wang, P., and Levelt, P. F.: Effective cloud fractions from the Ozone Monitoring Instrument: Theoretical framework and validation, J. Geophys. Res., 113, D16S38, doi:10.1029/2007JD008820, 2008.
Stavrakou, T., Müller, J.-F., De Smedt, I., Van Roozendael, M., van der Werf, G. R., Giglio, L., and Guenther, A.: Evaluating the performance of pyrogenic and biogenic emission inventories against one decade of space-based formaldehyde columns, Atmos. Chem. Phys., 9, 1037–1060, doi:10.5194/acp-9-1037-2009, 2009a.
Stavrakou, T., Müller, J.-F., De Smedt, I., Van Roozendael, M., van der Werf, G. R., Giglio, L., and Guenther, A.: Global emissions of non-methane hydrocarbons deduced from SCIAMACHY formaldehyde columns through 2003–2006, Atmos. Chem. Phys., 9, 3663–3679, doi:10.5194/acp-9-3663-2009, 2009b.
Stewart, D. J., Taylor, C. M., Reeves, C. E., and McQuaid, J. B.: Biogenic nitrogen oxide emissions from soils: impact on NO_x and ozone over west Africa during AMMA (African Monsoon Multidisciplinary Analysis): observational study, Atmos. Chem. Phys., 8, 2285–2297, doi:10.5194/acp-8-2285-2008, 2008.
Still, T. J., Al-Haider, S., Seakins, P. W., Sommariva, R., Stanton, J. C., Mills, G., and Penkett, S. A.: Ambient formaldehyde measurements made at a remote marine boundary layer site during the NAMBLEX campaign – a comparison of data from chromatographic and modified

ACPD
12, 7475–7520, 2012

Hantzsch techniques, Atmos. Chem. Phys., 6, 2711–2726, doi:10.5194/acp-6-2711-2006, 2006.
Stone, D., Evans, M. J., Commane, R., Ingham, T., Floquet, C. F. A., McQuaid, J. B., Brookes, D. M., Monks, P. S., Purvis, R., Hamilton, J. F., Hopkins, J., Lee, J., Lewis, A. C., Stewart, D., Murphy, J. G., Mills, G., Oram, D., Reeves, C. E., and Heard, D. E.: HO_x observations over West Africa during AMMA: impact of isoprene and NO_x, Atmos. Chem. Phys., 10, 9415–9429, doi:10.5194/acp-10-9415-2010, 2010.
Sumner, A. L., Shepson, P. B., Couch, T. L., Thornberry, T., Carroll, M. A., Sillman, S., Pippin, M., Bertman, S., Tan, D., Faloona, I., Brune, W., Young, V., Cooper, O., Moody, J., and Stockwell, W.: A study of formaldehyde chemistry above a forest canopy, J. Geophys. Res., 106, 24387–24405, doi:10.1029/2000JD900761, 2001.
Tao, Z., Larson, S. M., Wuebbles, D. J., Williams, A., and Caughey, M.: A summer simulation of biogenic contributions to ground-level ozone over the continental United States, J. Geophys. Res., 108, 4404, doi:10.1029/2002JD002945, 2003.
Taraborrelli, D., Lawrence, M. G., Crowley, J. N., Dillon, T. J., Gromov, S., Groß, C. B. M., Vereeckan, L., and Lelieveld, J.: Hydroxyl radical buffered by isoprene oxidation over tropical forests, Nat. Geosci., 5, 190–193, doi:10.1038/NGEO1405, 2012.
Torres, O., Tanskanen, A., Veihelmann, B., Ahn, C., Braak, R., Bhartia, P. K., Veefkind, P., and Levelt, P.: Aerosols and surface UV products from Ozone Monitoring Instrument observations: An overview, J. Geophys. Res., 112, D24S47, doi:10.1029/2007JD008809, 2007.
Trainer, M., Williams, E. J., Parrish, D. D., Buhr, M. P., Allwine, E. J., Westberg, H. H., Fehsenfeld, F. C., and Liu, S. C.: Models and observations of the impact of natural hydrocarbons on rural ozone, Nature, 329, 705–707, 1987.
Trentmann, J., Andreae, M. O., and Graf, H.-F.: Chemical processes in a young biomass-burning plume, J. Geophys. Res., 108, 4705, doi:10.1029/2003JD003732, 2003.
US EPA: Estimation Programs Interface for Windows Vista v4.10, US EPA, 2011.
van der Werf, G. R., Randerson, J. T., Giglio, L., Collatz, G. J., Kasibhatla, P. S., and Arellano Jr., A. F.: Interannual variability in global biomass burning emissions from 1997 to 2004, Atmos. Chem. Phys., 6, 3423–3441, doi:10.5194/acp-6-3423-2006, 2006.
Wang, Y., Jacob, D. J., and Logan, J. A.: Global simulation of tropospheric O_3-NO_x-hydrocarbon chemistry. 1. Model formulation, J. Geophys. Res., 103, 10713–10725, doi:10.1029/98JD00158, 1998.
Wesely, M. L.: Parameterization of surface resistances to gaseous dry deposition in

ACPD
12, 7475–7520, 2012

regional-scale numerical models, Atmos. Environ., 23, 1293–1304, 1989.
Yang, W., Shabanov, N. V., Huang, D., Wang, W., Dickinson, R. E., Nemani, R. R., Knyazikhin, Y., and Myneni, R. B.: Analysis of leaf area index products from combination of MODIS Terra and Aqua data, Remote Sens. Environ., 104, 297–312, 2006.
Yevich, R. and Logan, J. A.: An assessment of biofuel use and burning of agricultural waste in the developing world, Global Biogeochem. Cy., 17, 1095, doi:10.1029/2002GB001952, 2003.
Yienger, J. J. and Levy II, H.: Empirical model of global soil-biogenic NO_x emissions, J. Geophys. Res., 100, 11447–11464, doi:10.1029/95JD00370, 1995.
Zeng, X.: Global vegetation root distribution for land modeling, J. Hydrometeorol., 2, 525–530, 2001.

ACPD
12, 7475–7520, 2012

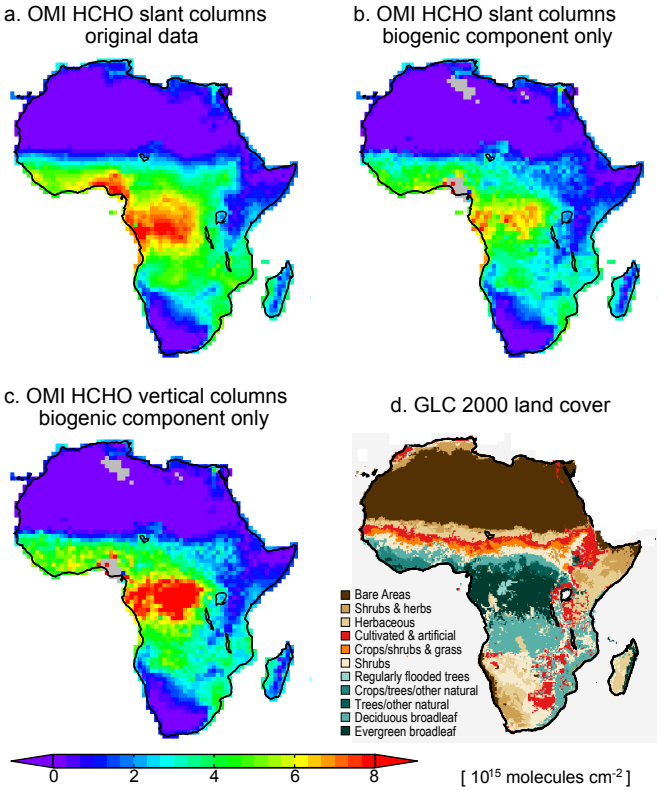

Fig. 1. HCHO columns and land cover types over Africa. The first three panels are annual mean HCHO columns for 2005–2009 at $1 \times 1^{\circ}$ resolution: **(a)** original slant columns, **(b)** biogenic slant columns after removing biomass burning, dust, and anthropogenic influences, **(c)** vertical columns obtained by applying air mass factors (AMFs) to the slant columns. The bottom right panel **(d)** shows the Global Land Cover (GLC) map for 2000 (Bartholomé and Belward, 2005).

ACPD
12, 7475–7520, 2012

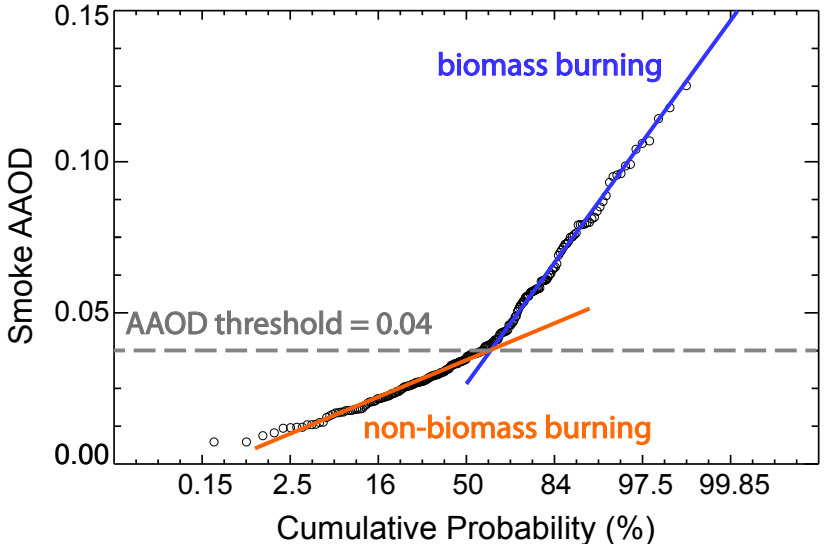

Fig. 2. Cumulative probability distribution of OMI smoke AAOD 8-day average values at $1 \times 1^{\circ}$ resolution over southern Africa (south of 2° S) for 2005–2009. The x-axis is a probability scale such that a normal distribution would plot as a straight line. This allows us to separate biomass burning from non-biomass burning conditions by plotting separate regression lines fitted to the bottom and top quantiles of the data. Intersection of these regression lines defines a smoke AAOD threshold for diagnosing biomass burning conditions and we remove the corresponding scenes from the OMI data set. Different AAOD thresholds are used for different regions of Africa as discussed in the text.

ACPD
12, 7475–7520, 2012

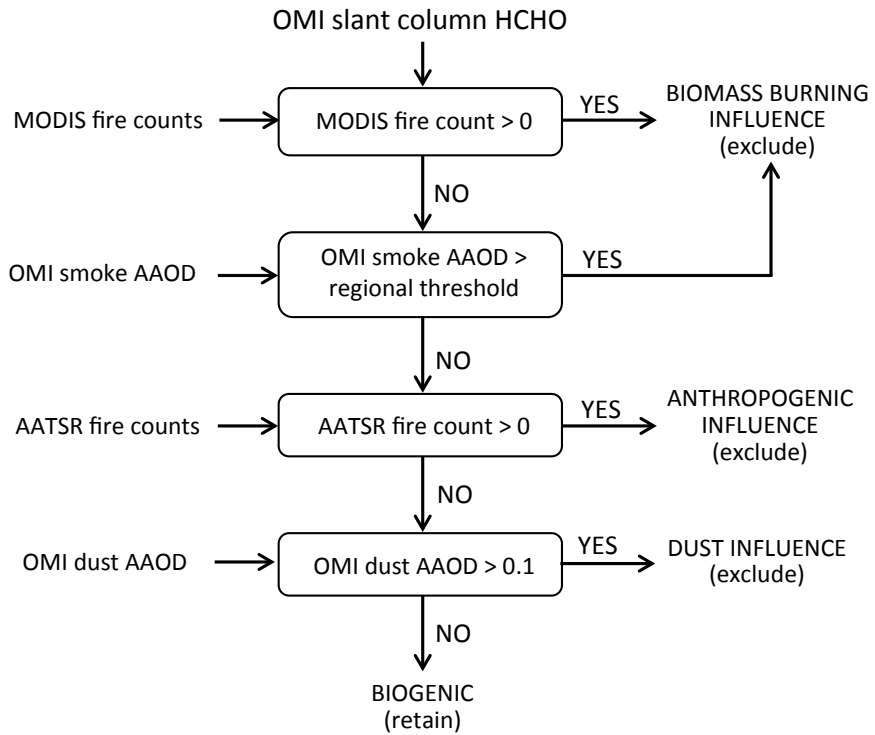

Fig. 3. Flow chart of the filtering algorithm used to remove biomass burning, dust, and anthropogenic influences in OMI slant HCHO columns (Ω_s). All data are 8-day averages on the same $1 \times 1^{\circ}$ grid. The MODIS fire counts filter uses MODIS data for the 8-day periods preceding and concurrent with the OMI HCHO observation.

ACPD
12, 7475–7520, 2012

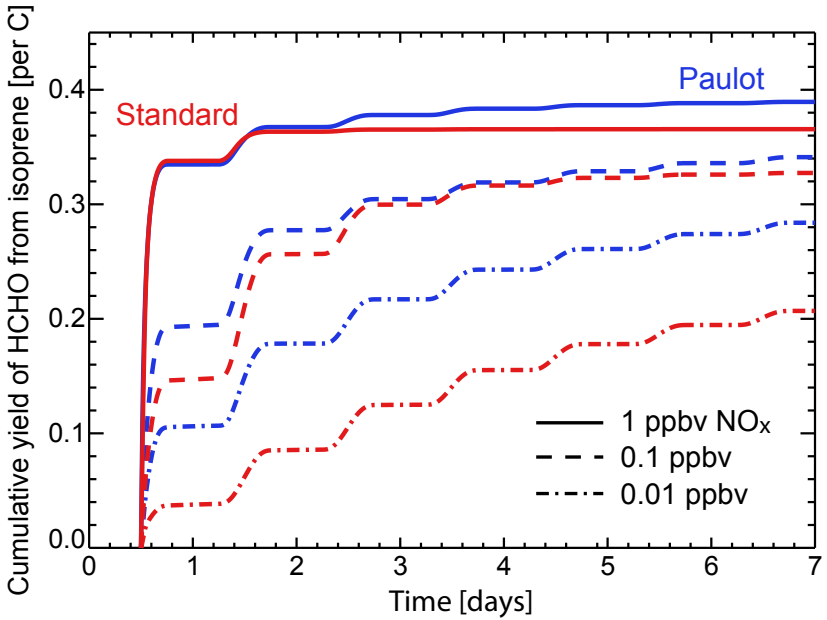

Fig. 4. Cumulative yields of HCHO per unit carbon from isoprene oxidation as a function of time in the DSMACC chemistry box model using the standard GEOS-Chem chemistry scheme (red) and the Paulot scheme (blue) for different NO_x levels and initialized at local noon. Details on the box model simulation are given in the text.

ACPD
12, 7475–7520, 2012

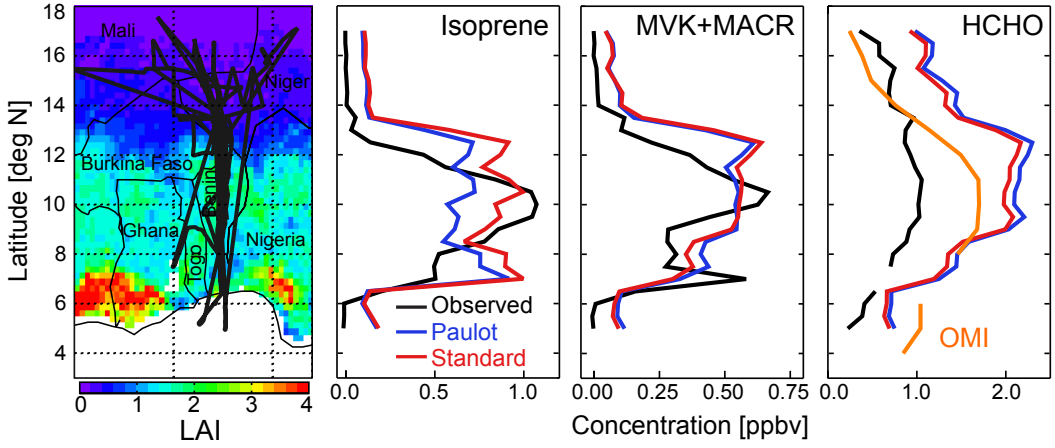

Fig. 5. Mean latitudinal gradients of boundary layer (>900 hPa) isoprene, MVK+MACR, and HCHO concentrations during the AMMA aircraft campaign in July–August 2006. The left panel shows the AMMA flight tracks superimposed on a map of MODIS leaf area index (LAI) (Yang et al., 2006) for the AMMA period. Observations averaged over 0.5° latitudinal bins are shown in black. Model results sampled along the flight tracks and at the flight times are shown in red (standard GEOS-Chem isoprene oxidation scheme) and in blue (Paulot scheme). Mean OMI HCHO averaged over 1° latitude bins for July–August 2005–2009 is shown in orange (see text).

ACPD
12, 7475–7520, 2012

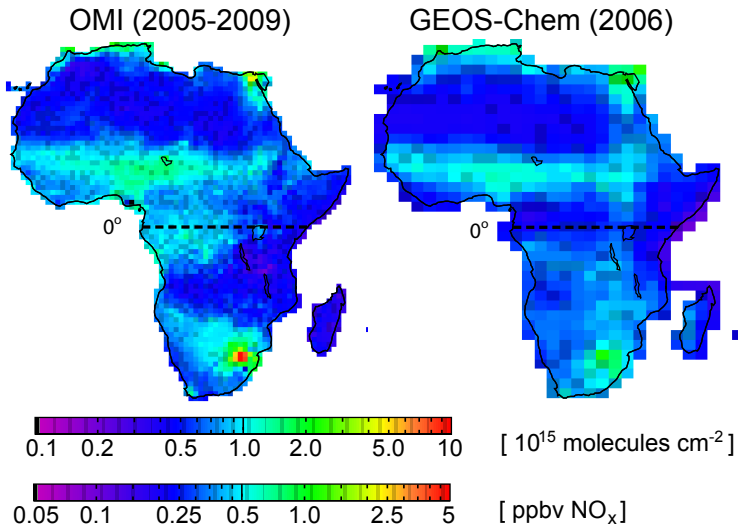

Fig. 6. Annual mean tropospheric NO_2 columns over Africa at 12:00–15:00 local time (LT). The left panel shows OMI 2005–2009 data at $1 \times 1^{\circ}$ resolution (Boersma et al., 2007). The right panel shows GEOS-Chem model values for 2006. The colorbar includes boundary layer (>900 hPa) NO_x estimated from column NO_2 (see text for details). Biomass burning influence was removed using MODIS fire counts and OMI smoke AAOD in the observations, and BC AOD in GEOS-Chem. The equator is indicated.

ACPD
12, 7475–7520, 2012

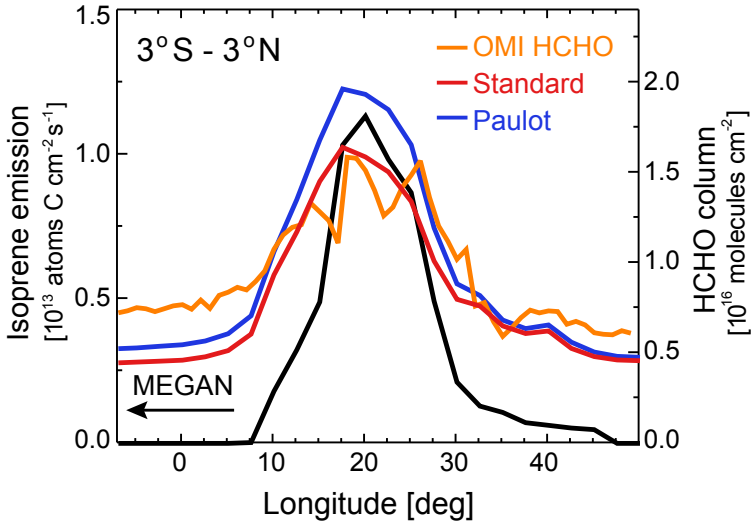

Fig. 7. Mean longitudinal gradients of isoprene emission (black) and HCHO columns (color) across central Africa (3° S–3° N) at 12:00–15:00 LT in July. HCHO columns are shown for the OMI observations in 2005–2009 (orange) and from the GEOS-Chem simulations using the standard isoprene oxidation scheme (red) and the Paulot scheme (blue) in 2006 at 12:00–15:00 LT. Isoprene emissions are from MEGAN. The HCHO columns have been filtered against biomass burning as described in the text.

ACPD
12, 7475–7520, 2012

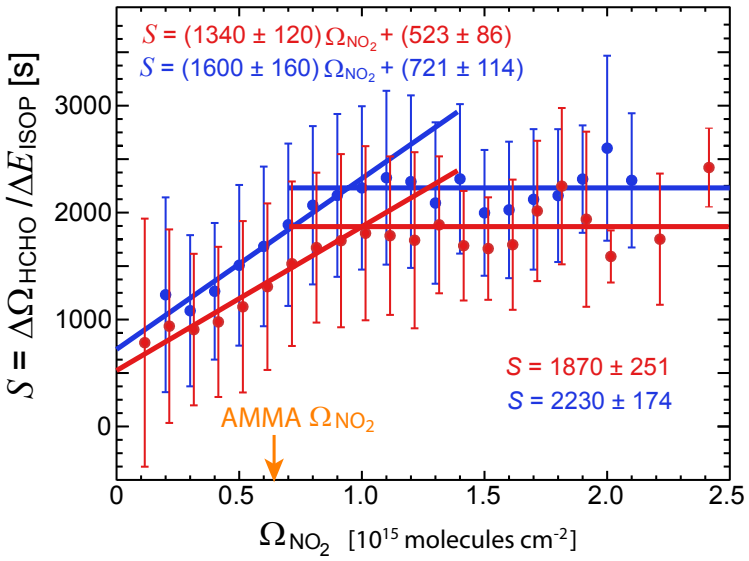

Fig. 8. Dependence of the HCHO-isoprene relationship on the local tropospheric NO_2 column Ω_{NO_2} over Africa in GEOS-Chem. The figure shows statistics of $S = \Delta\Omega_{HCHO}/\Delta E_{ISOP}$ computed as described in the text for individual $2 \times 2.5^{\circ}$ gridsquares and months in 2006 at 12:00–15:00 LT. Values of S have been sorted by the local value of Ω_{NO_2} in 1×10^{14} molecules cm^{-2} bins, and means and standard deviations are shown in each bin for GEOS-Chem using the standard isoprene oxidation scheme (red) and the Paulot scheme (blue). The data for $\Omega_{NO_2} \leq 1 \times 10^{15}$ molecules cm^{-2} show a linear relationship between S and Ω_{NO_2}, and reduced-major-axis regression parameters are shown inset with standard deviations determined using jackknife resampling (Manly, 1997). The data for $\Omega_{NO_2} > 1 \times 10^{15}$ molecules cm^{-2} show no significant dependence between S and Ω_{NO_2}, and the corresponding mean values and standard deviations of S are shown inset. The mean Ω_{NO_2} inferred from AMMA observations is also indicated (orange arrow).

ACPD
12, 7475–7520, 2012

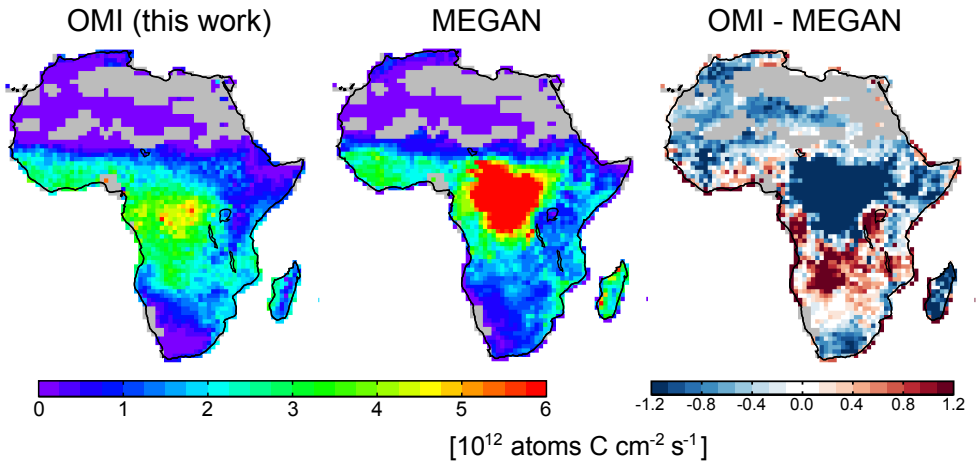

Fig. 9. Annual average isoprene emissions from Africa at $1 \times 1^{\circ}$ horizontal resolution at 12:00–15:00 LT. Values inferred from the OMI HCHO 2005–2009 data (left) are compared to values from the MEGAN bottom-up inventory (center). The right panel shows the difference between the two. Results are for the ensemble of $1 \times 1^{\circ}$ gridsquare-months that are not excluded from our analysis due to biomass burning, anthropogenic, dust, or smearing influences (see text). Completely excluded areas are shown in grey.

ACPD
12, 7475–7520, 2012